

Semiclassical Moyal quantum mechanics for atomic systems

B. R. McQuarrie, T. A. Osborn, and G. C. Tabisz

Department of Physics, University of Manitoba, Winnipeg, MB, Canada R3T 2N2

(Received 18 December 1997)

The Moyal formalism utilizes the Wigner transform and associated Weyl calculus to define a phase-space representation of quantum mechanics. In this context, the Weyl symbol image of the Heisenberg evolution operator admits a generic semiclassical expansion that is based on classical transport and related $O(\hbar^2)$ quantum corrections. For two atom systems with a mutual pair interaction described by a spherically symmetric potential, the predictive power and convergence properties of this semiclassical expansion are investigated via numerical calculation. The rotational invariance and tensor structure present are used to simplify the semiclassical dynamics to the point where numerical computation in the six-dimensional phase space is feasible. For a variety of initial Gaussian wave functions and a selection of different observables, the $O(\hbar^0)$ and $O(\hbar^2)$ approximations for time dependent expectation values are determined. The interactions used are the Lennard-Jones potentials, which model helium, neon, and argon. The numerical results obtained provide a first demonstration of the practicality and usefulness of Moyal quantum mechanics in the analysis of realistic atomic systems. [S1050-2947(98)08110-4]

PACS number(s): 03.65.Nk, 03.65.Sq, 34.50.-s

I. INTRODUCTION

Moyal quantum mechanics gives a complete statement of quantum theory that is set in classical phase space. It employs equations of motion that are similar to those of Hamiltonian mechanics. In this paper we study the predictive power and the computational usefulness of Moyal quantum mechanics (hereafter, MQM) in describing interatomic systems, specifically helium, neon, and argon. Although there is now an extensive literature which establishes the mathematical and structural aspects of MQM, this formalism has had limited application to, and interaction with, realistic physical systems. A remarkable feature of MQM is the simple structure assumed by the semiclassical expansion for the Heisenberg picture quantum flow. Through numerical calculation we investigate the convergence and the accuracy of this semiclassical expansion.

The Moyal formalism [1–30] is based on the Wigner-Weyl isomorphism that maps Hilbert space operators to functions (symbols) on classical phase space. The transformation of an operator \hat{A} on Hilbert space $\mathcal{H}=L^2(\mathbb{R}^3)$ to a corresponding Weyl symbol A on phase space $T^*(\mathbb{R}^3)\simeq\mathbb{R}_q^3\times\mathbb{R}_p^3$ is denoted $A=\sigma\hat{A}$. The map σ is defined by the Wigner transform [31],

$$A(q,p)=\int_{\mathbb{R}^3}dx e^{-ip\cdot x/\hbar}\langle q+\frac{1}{2}x|\hat{A}|q-\frac{1}{2}x\rangle. \quad (1.1)$$

In the integral above, $\langle x|\hat{A}|y\rangle$ denotes the coordinate space kernel of \hat{A} written in Dirac notation.

The inverse map σ^{-1} sends symbols to operators (Weyl quantization) [32] and is given by the inverse Fourier transform to Eq. (1.1). The map σ is a linear bijective correspondence. Observables (Hermitian operators) have real-valued symbols. If \hat{A} is the identity operator, then $A(q,p)=1$. The quantum position \hat{q}_j and momentum operators $\hat{p}_j\psi=-i\hbar\partial\psi/\partial q_j$ have as symbols the coordinate functions q_j and

p_j , respectively. Operator functions of $\hat{q}=(\hat{q}_1,\hat{q}_2,\hat{q}_3)$ alone or \hat{p} alone, say $f(\hat{q})$ or $g(\hat{p})$, have symbols $f(q)$ and $g(p)$.

Quantum flow in symbol space is the σ image of Heisenberg picture evolution. A system defined by a Hamiltonian operator \hat{H} has Schrödinger evolution $U(t)=\exp(-i\hat{H}t/\hbar)$ and an associated Heisenberg evolution operator $\Gamma(t)$. For a general observable \hat{A} , this is

$$\hat{A}(t)=\Gamma(t)\hat{A}\equiv U^\dagger(t)\hat{A}U(t). \quad (1.2)$$

The Weyl-symbol image of Eq. (1.2) replaces the pair of operators $\hat{A}(t), \hat{A}$ by their corresponding phase space symbols $A(t), A$. We refer to the linear transformation Γ_t from $A\mapsto A(t)$ as the Heisenberg-Weyl evolution operator. In view of the invertibility of σ , the operator Γ_t takes the form

$$A(t)=\Gamma_t A, \quad (1.3a)$$

$$\Gamma_t=\sigma\Gamma(t)\sigma^{-1}. \quad (1.3b)$$

The transformation Γ_t is the fundamental evolution operator in MQM.

The origin of semiclassical behavior for the Heisenberg-Weyl evolution arises from the notion of operators that are smooth in Planck's constant \hbar . A Hamiltonian \hat{H} is said to be semiclassically admissible if its symbol $H(\hbar,z)$ has a regular asymptotic expansion about $\hbar=0$,

$$H(\hbar,z)=H_c(z)+\sum_{r=1}^{\infty}\frac{\hbar^r}{r!}h_r(z). \quad (1.4)$$

In the notation above $z=(q,p)$ denotes a point in phase space. The \hbar -independent portion of the symbol $H(\hbar,z)$, namely, $H_c(z)$, is the classical counterpart of \hat{H} . Nearly all Hamiltonians of physically significant systems are semiclassically admissible. A system without higher order \hbar terms in Eq. (1.4) has the feature that the Weyl symbol $H(\hbar,z)$ is

exactly the classical Hamiltonian $H_c(z)$. Such systems are referred to as Weyl quantized.

In the circumstance wherein \hat{H} is semiclassically admissible, then Γ_t admits a small \hbar asymptotic expansion

$$\Gamma_t A \simeq \Gamma_t^{(N)} A \equiv \sum_{n=0}^N \frac{\hbar^n}{n!} \gamma_t^{(n)} A, \quad \hbar \downarrow 0. \quad (1.5)$$

The ‘‘coefficients’’ $\gamma_t^{(n)}$ associated with powers of \hbar are operators in the space of Weyl symbols. Expansion (1.5) is the generic (Heisenberg picture) form of semiclassical expansion [30] in MQM. The leading term $\gamma_t^{(0)}$ is determined by the classical flow in $T^*(\mathbb{R}^3)$ generated by H_c .

The final stage of the Moyal formalism obtains quantum expectation values. Let $\hat{\rho} = |\psi\rangle\langle\psi|$ be the density matrix for a unit normalized initial state $\psi \in \mathcal{H}$. The Wigner distribution is the σ image of $\hat{\rho}$, specifically $w_\psi = \hbar^{-3} \sigma \hat{\rho}$. The time dependent expectation for $\hat{A}(t)$ is determined via the trace formulas

$$\langle \hat{A}(t) \rangle_\psi = \text{Tr} \hat{\rho} \hat{A}(t) = \int dz w_\psi(z) \Gamma_t A(z) \quad (1.6a)$$

$$\simeq \int dz w_\psi(z) \Gamma_t^{(N)} A(z). \quad (1.6b)$$

Here the dz integral is over all phase space and Tr denotes the trace on \mathcal{H} .

For the physical systems considered in this paper the Hamiltonian \hat{H} has a symbol $H(\hbar, z)$ with a purely classical form

$$H(\hbar, z) = H_c(z) = \frac{p^2}{2m} + v(q). \quad (1.7)$$

The interatomic potential $v(q)$ will be the spherically symmetric phenomenologically determined Lennard-Jones interaction. The fact that $H(\hbar, z)$ is invariant under $\hbar \rightarrow -\hbar$ means that all the operators $\gamma_t^{(n)}$ with odd n vanish. This eliminates half of the semiclassical coefficients in (1.5). In this context the next quantum correction beyond the $\gamma_t^{(0)}$ term is $\gamma_t^{(2)}$.

This paper is organized as follows. Section II states the explicit formulas defining semiclassical flow operators $\Gamma_t^{(0)}$ and $\Gamma_t^{(2)}$ as they occur for static Hamiltonian systems. Section III shows how one may incorporate rotational invariance and tensor structure to obtain simplified systems of ordinary differential equations (ODE’s) for the functions required in the construction of the semiclassical flow operators. Section IV derives the reduced phase-space representations needed to calculate time dependent quantum expectation values for Gaussian initial wave functions. In Section V we summarize the computations that numerically implement the Moyal semiclassical expansion for systems that incorporate the interatomic potentials appropriate to helium, neon, and argon. The conclusions and related discussion are found in Sec. VI.

There are three appendices. Appendix A records the conventions and notations employed for the Weyl calculus [33] of phase-space functions. Also, one finds in Appendix A the

representations used to describe the noncommutative star product $*$ of symbols [2,19] as well as the semiclassical expansion of the Moyal bracket. Appendix B derives the phase space tensor structure of the Weyl calculus. Appendix C displays results that show how the various terms contributing to semiclassical expansion behave in phase space. This last appendix also describes some of the consistency tests employed to verify the correctness of the numerical calculations.

II. QUANTUM FLOW OPERATORS

The basic equations of motion for the flow operators $\Gamma_t^{(0)}$ and $\Gamma_t^{(2)}$ are reviewed in this section in sufficient detail to define these operators as solutions of a family of ordinary differential equations suitable for numerical calculation. In particular, we characterize the Jacobi field and quantum trajectory ingredients required to determine the semiclassical operators $\gamma_t^{(0)}$ and $\gamma_t^{(2)}$. Recent work of Osborn and Molzahn [30] has derived explicit formulas for $\gamma_t^{(n)}$ that are based on a connected graph representation of the exact evolution Γ_t . The following summary of this version of the Moyal formalism exploits the simplifications that result when the system has a static Hamiltonian and a static Schrödinger picture observable.

By and large, Refs. [1–35] cited for Moyal quantum mechanics are those papers that proved helpful in the development of the connected graph representation of Γ_t . A good overview of the large body of mathematical literature on this topic is found in the book [25] by Folland.

A. Moyal equation of motion

For a system \hat{H} and observable \hat{A} the Heisenberg picture equation of motion has the standard form

$$\frac{\partial}{\partial t} \Gamma(t) \hat{A} = \frac{1}{i\hbar} [\Gamma(t) \hat{A}, \hat{H}]. \quad (2.1)$$

Taking the Weyl symbol image of this yields the Moyal equation of motion,

$$\frac{\partial}{\partial t} \Gamma_t A = \{\Gamma_t A, H\}_M, \quad (2.2)$$

with initial condition $\Gamma_0 A = A$. The bracket of functions in Eq. (2.2) is the Moyal bracket, cf. Eq. (A4). A key feature of the bracket $\{\cdot, \cdot\}_M$ is that it has an ascending expansion in powers of \hbar , cf. Eq. (A8b), whose leading term is the Poisson bracket $\{\cdot, \cdot\}$.

The isomorphic nature of σ means that Γ_t acquires all the structural evolution properties of $\Gamma(t)$. As a result one has the following.

Properties of Γ_t . For all $t \in \mathbb{R}$, the evolution operator Γ_t (a) is linear on the space of symbols, (b) obeys the composition law: for all $\tau \in \mathbb{R}$, $\Gamma_t = \Gamma_{t-\tau} \Gamma_\tau$; (c) has inverse $\Gamma_t^{-1} = \Gamma_{-t}$; (d) maps the constant symbol into itself $\Gamma_t 1 = 1$; (e) commutes with the $*$ and Moyal bracket operations; for all symbols X, Y :

$$\Gamma_t(X * Y) = \Gamma_t(X) * \Gamma_t(Y), \quad \Gamma_t\{X, Y\}_M = \{\Gamma_t(X), \Gamma_t(Y)\}_M.$$

The semiclassical approximation $\Gamma_t^{(N)}$ mirrors the Γ_t evolution properties to order $O(\hbar^{N+2})$. In detail, properties (b), (c), and (e) are valid to order $O(\hbar^{N+2})$, while features (a) and (d) remain exact. The fact that (d) holds implies that the flow $\Gamma_t^{(N)}$ conserves wave function norm. This statement is verified by noting that the identity operator $\hat{A}=I$ gives the probability expectation value, $\|\psi\|^2 = \text{Tr } \hat{A}|\psi\rangle\langle\psi|$. Now observe that $\gamma_t^{(0)}1=1$ and $\gamma_t^{(n)}1=0$, $n \geq 1$. This latter identity follows from the derivative nature of $\gamma_t^{(n)}$, $n \geq 1$ [cf. Eq. (2.11)]. Thus

$$\int dz \Gamma_t^{(N)} w_\psi(z) = \int dz w_\psi(z) \Gamma_t^{(N)} 1 = \int dz w_\psi(z) = \|\psi\|^2. \quad (2.3a)$$

The work of Antonets [13,14] has established that the exact Heisenberg-Weyl evolution Γ_t converges to the semiclassical evolution $\Gamma_t^{(0)}$ in the limit $\hbar \downarrow 0$. For a class of observables, namely, $A \in C_0^\infty(\mathbb{R}^6)$, and any finite time interval $[0, T]$ it was proved that [13]

$$\|[\Gamma_t - \Gamma_t^{(0)}]A\|_{L^2(\mathbb{R}^6)} < \hbar^2 C(T, A), \quad t \in [0, T]. \quad (2.3b)$$

The exposed factor of \hbar^2 arises from the difference of the Moyal and the Poisson bracket, cf. (A8b). The constant $C(T, A)$ is a growing function of time T . More recent work [34] on error bounds estimates the difference $\|[\Gamma_t - \Gamma_t^{(0)}]A\|$ and studies how the bounding constant $C(T, A)$ behaves for large T .

B. First-order semiclassical flow

Let \hat{H} be the Weyl quantized Hamiltonian, $\hat{H} = \sigma^{-1}H_c$. From now on we drop the ubiquitous subscript c found on H_c . If \hat{A} is a semiclassically admissible operator with an \hbar independent symbol, the $O(\hbar^0)$ part of Eq. (2.2) is seen to be

$$\frac{\partial}{\partial t} \Gamma_t^{(0)} A(z) = \{\Gamma_t^{(0)} A, H\}(z). \quad (2.4a)$$

One immediately recognizes Eq. (2.4a) as a Poisson bracket equation of motion for the unknown phase space function $\Gamma_t^{(0)} A$.

As is well known, Eq. (2.4a) may be solved via classical transport. Specifically, let $g(t|z)$ be the classical flow defined as a solution to Hamilton's equation,

$$\frac{d}{dt} g(t|z) = J \nabla H(g(t|z)). \quad (2.4b)$$

Here ∇H denotes the phase space gradient $(\nabla_q H, \nabla_p H)$ and J is the Poisson matrix, cf. Eq. (A3), responsible for the symplectic structure of Hamiltonian mechanics. The initial condition for (2.4b) is $g(0|z) = z$. The flow $g(t)$ preserves phase-space volume and is defined for all t . Given the classical flow $g(t)$, the solution of Eq. (2.4a) is the composition

$$\Gamma_t^{(0)} A(z) = A(g(t|z)) = [A \circ g(t)](z). \quad (2.5)$$

As is evident, $\Gamma_t^{(0)} A$ acquires its time dependence via the classical motion $g(t)$. In this sense the flow operator $\Gamma_t^{(0)}$ is

trivial to calculate. Although $\Gamma_t^{(0)}$ is determined by $g(t)$, this $O(\hbar^0)$ version of semiclassical dynamics is not pure classical mechanics. In the evaluation of expectation values via Eq. (1.6b) complex valued wave functions and associated interference effects are fully present. What is absent, at this $\Gamma_t^{(0)}$ level of approximation, are the noncommutative effects of the $*$ product.

C. Higher-order semiclassical flow

Although the operator $\gamma_t^{(2)}$ is also a function of the flow $g(t)$ its construction requires a number of auxiliary functions. The basic form of $\gamma_t^{(2)}$ is determined as a consequence of the \hbar expansion of Γ_t in Eq. (1.5) combined with the \hbar expansion of the Moyal bracket. The connected graph based formula for $\gamma_t^{(2)}$ has the following characterization.

The operator $\gamma_t^{(2)}$ is defined via two basic ingredients—the Jacobi field [35] along the trajectory $g(t|z)$ and the notion of a quantum trajectory. Consider first the relevant Jacobi fields. Jacobi fields describe the stability of a trajectory with respect to small modifications of its initial data. Differentiating (2.4b) in the parameter z gives

$$\mathcal{J}(t) \nabla g(t|z) \equiv \left[\frac{d}{dt} - J \nabla \nabla H(g(t|z)) \right] \nabla g(t|z) = 0. \quad (2.6)$$

The solutions $f(t)$ to the homogeneous equation $\mathcal{J}(t)f(t) = 0$ are called Jacobi fields. The 6×6 matrix $\nabla g(t|z)$ obeys the initial condition $\nabla g(0|z) = \delta$ (the identity matrix) and each column is a Jacobi field. For all t and z , $\nabla g(t|z)$ is a symplectic matrix and thereby $\det \nabla g(t|z) = 1$. This latter fact is a statement of the incompressible nature of classical flow and ensures that the matrix $\nabla g(t|z)$ has a nonsingular inverse—namely, that there are no caustics.

The notion of a quantum trajectory arises from computing the Heisenberg-Weyl flow of the coordinate functions $z = (q, p) = (z_1, \dots, z_6)$,

$$Z_\mu(t, \hbar; z) \equiv \Gamma_t z_\mu. \quad (2.7)$$

The coordinate functions are semiclassically admissible and so Z_μ admits the standard asymptotic expansion in \hbar

$$Z_\mu(t, \hbar; z) = g_\mu(t|z) + \frac{\hbar^2}{2} z_\mu^{(2)}(t|z) + O(\hbar^4). \quad (2.8)$$

The coefficient function $z_\mu^{(2)}(t|z)$ obeys [30] an inhomogeneous Jacobi equation,

$$\begin{aligned} \mathcal{J}(t)_{\mu\nu} z_\nu^{(2)}(t|z) = & -\frac{1}{8} w_{\alpha\beta}(t|z) J_{\mu\gamma} H_{;\alpha\beta\gamma}(g(t|z)) \\ & + \frac{1}{12} w_{\alpha\beta\gamma}(t|z) J_{\mu\rho} H_{;\alpha\beta\gamma\rho}(g(t|z)) \end{aligned} \quad (2.9)$$

with initial condition $z_\mu^{(2)}(0|z) = 0$. The right-hand side of Eq. (2.9) utilizes tensor notation for derivatives, namely $H_{;\alpha\beta}$ denotes the α, β matrix element of the Hessian $\nabla \nabla H$, etc. Unless otherwise noted we employ the tensor summation convention on repeated indices. The Greek indices $\alpha\beta \cdots \nu$ run from 1 to 6. Furthermore, the expressions involving tensors $w_{\alpha\beta}$ and $w_{\alpha\beta\gamma}$ are defined as

$$w_{\alpha\beta}(t|z) = B_{12}^2 \langle g_\alpha(t), g_\beta(t) \rangle(z), \quad (2.10a)$$

$$\begin{aligned} w_{\alpha\beta\gamma}(t|z) &= B_{12}B_{23} \langle g_\alpha(t), g_\beta(t), g_\gamma(t) \rangle(z) \\ &= -J\nabla g_\alpha(t|z) \cdot \nabla \nabla g_\beta(t|z) J\nabla g_\gamma(t|z). \end{aligned} \quad (2.10b)$$

The derivative operators B_{ij} are the extended Poisson bracket operators that appear in the \hbar -expansion of the Moyal bracket, cf. Appendix A. It is often useful to decompose both $g(t|z)$ and $z^{(2)}(t|z)$ into their coordinate and momentum parts. For trajectories we write $g(t|z) = (q(t|z), p(t|z))$. Similarly $z^{(2)}(t|z)$ breaks into $q^{(2)}(t|z)$ and $p^{(2)}(t|z)$.

Once $z^{(2)}(t|z)$ has been determined from the solution of Eq. (2.9), the semiclassical flow operator $\gamma_t^{(2)}$ is given by the expression

$$\begin{aligned} \gamma_t^{(2)} A(z) &= z_\alpha^{(2)}(t|z) A_{;\alpha}(g(t|z)) - \frac{1}{8} w_{\alpha\beta}(t|z) A_{;\alpha\beta}(g(t|z)) \\ &\quad + \frac{1}{12} w_{\alpha\beta\gamma}(t|z) A_{;\alpha\beta\gamma}(g(t|z)). \end{aligned} \quad (2.11)$$

A number of comments about the nature of $\gamma_t^{(2)}$ are in order. Expression (2.11) defines a linear operator on a smooth symbol A . It is globally defined throughout phase space for all time t . Each of the terms in Eq. (2.11) follows the classical trajectory $g(t|z)$. Finally, Eq. (2.11) is also seen to be a derivative expansion in the z dependence of A . The analysis establishing Eq. (2.11) is found in Ref. [30]. The connected graph character of this formula is evident from equations (2.10a) and (2.10b). The $w_{\alpha\beta}$ term is composed of two vertex functions g_α, g_β , which are linked by two copies of the edge operator B_{12} . The $w_{\alpha\beta\gamma}$ term is a tree graph on the vertices $g_\alpha, g_\beta, g_\gamma$ with edges B_{12}, B_{23} . In Appendix A formula (2.11) is verified by deriving it with a technique that does not employ the connected graph method of Ref. [30].

III. SYMMETRIES AND CONSTANTS OF MOTION

The presence of symmetries at either the quantum or the classical level simplifies the calculation of dynamics. The main symmetry for the interatomic Hamiltonian (1.7) is angular momentum conservation. Most observables and dynamical quantities such as the quantum trajectories and Jacobi fields are tensors. In this section, we determine the tensor character and rotational invariance properties of all the ingredients of the semiclassical expansion.

Let $\hat{L}_j \equiv \epsilon_{jkm} \hat{q}_k \hat{p}_m$ denote the j th component of the angular momentum operator in \mathcal{H} . The Weyl symbol of this operator is $L_j \equiv \epsilon_{jkm} q_k p_m$. The hypothesis of rotational invariance stated in both the operator and symbol form is

$$[\hat{H}, \hat{L}_j] = 0, \quad (3.1a)$$

$$\{H, L_j\}_M = \{H, L_j\} = 0. \quad (3.1b)$$

The vanishing of the commutator (3.1a) requires that the Moyal bracket in Eq. (3.1b) be zero. The equality of the Moyal and Poisson brackets results from the z -quadratic form of L_j . Specifically, all higher-order terms in the \hbar expansion of $\{H, L_j\}_M$ are zero.

A. Trajectory tensor structure

Consider the quantum trajectory defined in Eq. (2.7). Each coordinate rotation $q \mapsto q' = Rq$ with $R = R_n(\phi)$ defines a point canonical phase space rotation $z \mapsto z' = \mathcal{R}z = (Rq, Rp)$, cf. Appendix B. The first basic assertion is that the set of functions $\{Z_\mu(t, \hbar; z); \mu = 1-6\}$ transforms as a rank one phase-space tensor under rotation \mathcal{R} ,

$$Z_\mu(t, \hbar; \mathcal{R}z) = \mathcal{R}_{\mu\nu} Z_\nu(t, \hbar; z). \quad (3.2a)$$

Putting the semiclassical expansions (2.8) into Eq. (3.2a) shows that the \hbar -coefficient symbols are also rank one tensors, namely,

$$g_\mu(t|\mathcal{R}z) = \mathcal{R}_{\mu\nu} g_\nu(t|z), \quad (3.2b)$$

$$z_\mu^{(n)}(t|\mathcal{R}z) = \mathcal{R}_{\mu\nu} z_\nu^{(n)}(t|z). \quad (3.2c)$$

In order to verify the claim (3.2a) first note that quantum evolution $U(t)$ and unitary rotation $U(R)$ commute. Now conjugate $\Gamma(t)\hat{z}$ with $U(R)$ to obtain

$$\begin{aligned} U^\dagger(R) (\Gamma(t)\hat{z}_\mu) U(R) &= \Gamma(t) (U^\dagger(R)\hat{z}_\mu U(R)) \\ &= \mathcal{R}_{\mu\nu} (\Gamma(t)\hat{z}_\nu). \end{aligned} \quad (3.3)$$

The second equality above uses the metaplectic identity (B3). Equation (3.3) shows that $\Gamma(t)\hat{z}$ is a rank one (operator valued) phase-space tensor. Applying the Weyl symbol tensor transformation rules (B6) and (B7) establishes Eq. (3.2a).

Observe that transform (3.2b) for classical trajectories may be obtained directly from $\{H, L_j\} = 0$ in combination with Hamilton's equation of motion. The geometrical meaning of Eq. (3.2) is that both the classical trajectory and the quantum corrections act as rigid objects under the rotation \mathcal{R} .

An important simplifying feature of classical motion, which conserves angular momentum, is that trajectories lie in a two-dimensional plane. So it is useful to find the Moyal equivalent of this property. Let $\hat{L}_j(t) = \Gamma(t)\hat{L}_j$ denote the Heisenberg evolution of \hat{L}_j . Commutation of \hat{L} and \hat{H} implies that $\hat{L}_j(t) = \hat{L}_j(0) = \hat{L}_j$. The quantum planar motion restriction is

$$\hat{q}(t) \cdot \hat{L} = 0, \quad \hat{p}(t) \cdot \hat{L} = 0. \quad (3.4)$$

Identities (3.4) result when the skew symmetric tensor ϵ_{jkm} is contracted into a $j \leftrightarrow k$ symmetric product $\hat{q}_j(t)\hat{q}_k(t)$, etc.

Take the Wigner transform of Eq. (3.4) and expand the result in powers of \hbar . The leading $O(\hbar^0)$ contribution is given by the algebraic product of symbols and upon utilizing Eq. (2.8) is obviously

$$L_j(g(t|z)) = L_j(z), \quad (3.5a)$$

$$q(t|z) \cdot L(z) = 0, \quad (3.5b)$$

$$p(t|z) \cdot L(z) = 0. \quad (3.5c)$$

These results are purely classical. They state the planar motion restriction for the trajectory $g(t|z)$. Next calculate

the $O(\hbar^n)$ identities generated by Eq. (3.4). For this purpose it is helpful to note that the $*$ product with L is a truncated \hbar series. For any smooth symbol f

$$f * L_j(z) = f(z)L_j(z) + \frac{i\hbar}{2} \{f, L_j\}(z) + \frac{\hbar^2}{4} \epsilon_{jkm} \frac{\partial^2 f(z)}{\partial p_k \partial q_m}. \quad (3.6)$$

In the present application f is either $\sigma(\hat{q}(t))$ or $\sigma(\hat{p}(t))$. The $O(\hbar^1)$ contribution is proportional to $\{q_j(g(t)), L_j(g(t))\}(z) = \{q_j, L_j\} \circ g(t|z)$. Since $\{q_j, L_j\} = 0$, this term vanishes. The $O(\hbar^2)$ term has contributions from the last factor in Eq. (3.6) and the $z^{(2)}(t|z)$ part of Eq. (2.8) altogether giving

$$q^{(2)}(t|z) \cdot L(z) = -\frac{1}{2} \epsilon_{jkm} \frac{\partial^2 q_j(t|z)}{\partial p_k \partial q_m}, \quad (3.7a)$$

$$p^{(2)}(t|z) \cdot L(z) = -\frac{1}{2} \epsilon_{jkm} \frac{\partial^2 p_j(t|z)}{\partial p_k \partial q_m}. \quad (3.7b)$$

These identities impose a constraint on the allowed forms of $q^{(2)}(t|z)$ and $p^{(2)}(t|z)$.

B. Jacobi field symmetries

In this subsection we develop representations of the Jacobi field tensor $\nabla g(t|z)$ and $\nabla \nabla g(t|z)$, which exploit the planar motion and rotational invariance of the classical trajectories. The goal is to obtain reduced equations of motion for these tensors that are suitable for numerical calculation. For example, rotational invariance allows $\nabla g(t|z)$ to be block diagonalized and described by 20 nonzero tensor components instead of the 36 components that a general rank 2 tensor requires.

First, it is useful to have a coordinate description of $T^*(\mathbb{R}_q^3)$ that incorporates the maximum scalar structure. Let $\{e_i; i=1-3\}$ be a right-handed orthogonal basis for \mathbb{R}_q^3 . A standard [36] fixed axis Euler angle representation of \mathbb{R}^3 rotation is $R(\alpha, \beta, \gamma) = R_{e_3}(\alpha)R_{e_2}(\beta)R_{e_3}(\gamma)$. In terms of the α, β, γ variables the \mathcal{R} rotation of an initial phase space point $z_0 = (q_0, p_0)$ becomes

$$q = R(\alpha, \beta, \gamma)q_0, \quad p = R(\alpha, \beta, \gamma)p_0. \quad (3.8a)$$

The three \mathcal{R} invariant scalars formed from q, p are evidently

$$|q| = |q_0| \equiv r, \quad |p| = |p_0| \equiv p_r, \quad q \cdot p = q_0 \cdot p_0 = r p_r \cos \theta. \quad (3.8b)$$

Here θ is the opening angle between the vectors q_0 and p_0 . Note that the three vectors $q_0, p_0, q_0 \times p_0$ define a rigid body and that transform (3.8a) rotates that body into all possible orientations. The scalar variables r, p_r, θ may be interpreted as characterizing the ‘‘internal’’ geometrical structure of this rigid body. For convenience we select the coordinate system $\{e_i\}$ so that $e_3 = q_0 \times p_0 / |q_0 \times p_0|$ and $e_2 = p_0 / |p_0|$. In terms of the scalar invariants the point z_0 is then represented by

$$q_0 = (r \sin \theta) e_1 + (r \cos \theta) e_2, \quad \theta \in [0, \pi); \quad p_0 = p_r e_2. \quad (3.8c)$$

In combination (3.8a) and (3.8c) provide a Euler angle, scalar invariant coordinatization of phase space, $z = z(\alpha, \beta, \gamma, r, p_r, \theta)$. As a shorthand notation, we often refer to the e_1 - e_2 plane as the z_0 plane.

The Jacobi field $[\nabla g(t|z)]_{\mu\lambda} = g_{\mu;\lambda}$ and the related function $[\nabla \nabla g(t|z)]_{\mu\lambda\rho} = g_{\mu;\lambda\rho}$ are rank 2 and rank 3 tensors, respectively. Thus if one determines $g_{\mu;\lambda}$ on the z_0 plane, it may be extended to all $z = \mathcal{R}z_0$ by

$$g_{\mu;\lambda}(t|z) = \mathcal{R}_{\mu\mu'}(\alpha, \beta, \gamma) \mathcal{R}_{\lambda\lambda'}(\alpha, \beta, \gamma) g_{\mu';\lambda'}(t|z_0). \quad (3.9)$$

A similar relationship holds for $g_{\mu;\lambda\rho}$.

In view of Eq. (3.9) we may restrict, without loss of generality, the numerical calculation of ∇g and $\nabla \nabla g$ to the z_0 plane. In this plane these tensors can be block diagonalized in the following fashion. Let V'' denote the Hessian of v , whose ij th matrix element is

$$V_{ij}(q) = \left(\frac{v''(r)}{r^2} - \frac{v'(r)}{r^3} \right) q_i q_j + \frac{v'(r)}{r} \delta_{ij}. \quad (3.10a)$$

With this notation the Jacobi field equation (2.6) for $\nabla g(t|z_0)$ reads

$$\left[\frac{d}{dt} + \begin{pmatrix} 0 & -m^{-1}\delta \\ V'' & 0 \end{pmatrix} \right] \begin{pmatrix} Y_{\cdot\lambda}(t|z_0) \\ W_{\cdot\lambda}(t|z_0) \end{pmatrix} = 0, \quad \lambda = 1-6. \quad (3.10b)$$

In Eq. (3.10b) we have named the top half 3×6 portion of $\nabla g(t|z_0)$ as $Y(t|z_0)$ and the lower half as $W(t|z_0)$. From Eq. (3.10b) one has immediately that $W(t|z_0) = m\dot{Y}(t|z_0)$. Using this last relation, the equation for Y becomes

$$\left[m \frac{d^2}{dt^2} + V''(q(t|z_0)) \right] Y_{\cdot\lambda}(t|z_0) = 0 \quad (3.10c)$$

with initial conditions $Y_{i\lambda}(0|z_0) = \delta_{i\lambda}$, $\dot{Y}_{i\lambda}(0|z_0) = m^{-1} \delta_{i+3,\lambda}$.

Next consider the symmetry based simplifications of Eq. (3.10c). The classical trajectory $g(t|z_0)$ remains in the z_0 plane and so $g_3(t|z_0) = g_6(t|z_0) = 0$. Thus the Hessian of the potential is block diagonalized as

$$V''(q(t|z_0)) = \begin{pmatrix} V_{11} & V_{12} & 0 \\ V_{21} & V_{22} & 0 \\ 0 & 0 & V_{33} \end{pmatrix}. \quad (3.10d)$$

As a result (3.10c) decouples into two parts

$$\left[m \frac{d^2}{dt^2} + \begin{pmatrix} V_{11} & V_{12} \\ V_{12} & V_{22} \end{pmatrix} \right] \begin{pmatrix} Y_{1\lambda}(t|z_0) \\ Y_{2\lambda}(t|z_0) \end{pmatrix} = 0, \quad (3.10e)$$

$$\left[m \frac{d^2}{dt^2} + V_{33} \right] Y_{3\lambda}(t|z_0) = 0. \quad (3.10e)$$

Equations (3.10e) are homogeneous second-order ODE's for $Y(t|z_0)$. Note that if $\lambda = 3, 6$ while $i = 1, 2$ then $Y_{i\lambda}(t|z_0) = 0$. This is a consequence of the initial condition

$Y_{i\lambda}(0|z_0) = \dot{Y}_{i\lambda}(0|z_0) = 0$. For similar reasons, if $\lambda = 1, 2, 4, 5$ and $i = 3$, a zero valued solution occurs. In matrix form we have

$$Y(t|z_0) = \begin{pmatrix} g_{1;1} & g_{1;2} & 0 & g_{1;4} & g_{1;5} & 0 \\ g_{2;1} & g_{2;2} & 0 & g_{2;4} & g_{2;5} & 0 \\ 0 & 0 & g_{3;3} & 0 & 0 & g_{3;6} \end{pmatrix}. \quad (3.10f)$$

The lower half of $\nabla g(t|z)$ is recovered from $W(t|z_0) = m\dot{Y}(t|z_0)$. From Eq. (3.10e) all 36 values of $g_{\mu;\lambda}(t|z_0)$ may be efficiently computed. The planar motion symmetry has forced 16 of the tensor values to be zero.

To find the optimal decoupled equations for $\nabla\nabla g(t|z_0)$ return to Eq. (3.10c) and take the z_0 derivative of that equation. Then proceeding as above one obtains

$$\left[m \frac{d^2}{dt^2} + \begin{pmatrix} V_{11} & V_{12} \\ V_{21} & V_{22} \end{pmatrix} \right] \begin{pmatrix} Y_{1\lambda\rho}(t|z_0) \\ Y_{2\lambda\rho}(t|z_0) \end{pmatrix} = - \begin{pmatrix} V_{1jk} Y_{j\lambda} Y_{k\rho} \\ V_{2jk} Y_{j\lambda} Y_{k\rho} \end{pmatrix}, \quad (3.11a)$$

$$\left[m \frac{d^2}{dt^2} + V_{33} \right] Y_{3\lambda\rho}(t|z_0) = -V_{3jk} Y_{j\lambda} Y_{k\rho}. \quad (3.11b)$$

Here $Y_{i\lambda\rho} = g_{i;\lambda\rho}$ and the jk tensor contractions run over the 1–3 index set. The initial conditions are $Y_{i\lambda\rho}(0|z_0) = \dot{Y}_{i\lambda\rho}(0|z_0) = 0$. Given $Y_{i\lambda\rho}$ for $i = 1-3$ the momentum type fields g_{i+3} are determined by $g_{i+3;\lambda\rho} = m\dot{Y}_{i\lambda\rho}$. Equations (3.11a) and (3.11b) require the third derivative of the potential. This is

$$V_{ijk} = \left(\frac{v'''(r)}{r^3} - \frac{3v''(r)}{r^4} + \frac{3v'(r)}{r^5} \right) q_i q_j q_k + \left(\frac{v''(r)}{r^2} - \frac{v'(r)}{r^3} \right) (q_i \delta_{jk} + q_j \delta_{ik} + q_k \delta_{ij}). \quad (3.11c)$$

Rotational invariance causes many of the components of $\nabla\nabla g(t|z_0)$ to be zero. Let us first record this pattern of zeros and then analyze how they arise from Eq. (3.11). To assist in representing $\nabla\nabla g$, introduce a partition of the index set 1–6 into $A = (1, 2, 4, 5)$ and $B = (3, 6)$. Indices A describe the allowed e_1 - e_2 planar variables while the set B is associated with the direction e_3 . For each given μ , $\nabla\nabla g_\mu$ is a 6×6 symmetric matrix with entries $g_{\mu;\lambda\rho}$. Reorder the rows and columns of $\nabla\nabla g_\mu$ by the index transformation $\mathcal{I}(1-6) = (1, 2, 4, 5, 3, 6)$ and denote the \mathcal{I} transformed representation by $\mathcal{I}\nabla\nabla g_\mu \mathcal{I}^{-1}$. In block matrix form

$$\mathcal{I}\nabla\nabla g_\mu \mathcal{I}^{-1} = \begin{bmatrix} X_{aa}^\mu & X_{ab}^\mu \\ X_{ba}^\mu & X_{bb}^\mu \end{bmatrix}. \quad (3.12a)$$

Here X_{ab}^μ is the 4×2 rectangular matrix on the indices $A \times B$, etc. The $\mathcal{I}\nabla\nabla g_\mu \mathcal{I}^{-1}$ matrix has two forms depending on the index μ ,

$$\begin{bmatrix} X_{aa}^\mu & 0 \\ 0 & X_{bb}^\mu \end{bmatrix}, \quad \mu \in A \quad (3.12b)$$

and

$$\begin{bmatrix} 0 & X_{ab}^\mu \\ X_{ba}^\mu & 0 \end{bmatrix}, \quad \mu \in B.$$

So the tensor $\nabla\nabla g(t|z_0)$ with 216 entries has 112 nonzero values. The transpose symmetry $X_{aa}^\mu = X_{aa}^{\mu T}$, $X_{bb}^\mu = X_{bb}^{\mu T}$, and $X_{ab}^\mu = X_{ba}^{\mu T}$ implies there are only 68 distinct time dependent functions $g_{\mu;\lambda\rho}(t|z_0)$.

The basic mechanism that forces $Y_{i\lambda\rho}$ to be zero is simple. The vanishing initial values of $Y_{i\lambda\rho}(0|z_0)$ and $\dot{Y}_{i\lambda\rho}(0|z_0)$ mean that the solutions of the second-order ODE's Eqs. (3.11a) and (3.11b) are nonzero only if the RHS inhomogeneous term is nonzero. Thus it suffices to catalog the index values $i\lambda\rho$ for which the term $V_{ijk} Y_{j\lambda} Y_{k\rho}$ is zero. To begin, observe that the third derivative $V_{ijk}(q(t|z_0))$ is zero if one of the three indices is 3 while the other two are in (1, 2). Also note that $V_{333}(q(t|z_0)) = 0$. The zero values of $Y(t|z_0)$, as seen in Eq. (3.10f), when combined with the V_{ijk} behavior above show that $V_{ijk} Y_{j\lambda} Y_{k\rho}$ vanishes in two different situations. Case I: for $i = 1-2$ where the pair $\lambda\rho$ are disjointly assigned to A and B . Case II: for $i = 3$ where the pair $\lambda\rho$ are either both in A or in B . These two cases produce the zero block structure displayed in Eq. (3.12b).

C. Equation of motion for $z^{(2)}(t|z_0)$

Having obtained, for a given trajectory $g(t|z_0)$, the associated values of $\nabla g(t|z_0)$ and $\nabla\nabla g(t|z_0)$ from the solutions of Eqs. (3.10c) and (3.11) one has all the functions required to determine $z^{(2)}(t|z_0)$. At this stage it is useful to have a symmetry reduced form of the inhomogeneous Jacobi equation (2.9) for the unknown $z^{(2)}(t|z_0)$.

The planar motion invariance implies that to order $O(\hbar^2)$ the quantum trajectory stays in the classical plane of motion. In order to verify this claim note that $L(z_0) = L_3(z_0)e_3$ so that the constraint condition (3.7a) reads

$$q_3^{(2)}(t|z_0)L_3(z_0) = (Y_{1;53} - Y_{1;62}) + (Y_{2;61} - Y_{2;43}) + (Y_{3;42} - Y_{3;51}). \quad (3.13)$$

The first four Y terms are in case I above, while the last two are in case II. So all terms on the right side of Eq. (3.13) vanish. Since $L_3(z_0) \neq 0$ for $\theta \in (0, \pi)$ we have that $q_3^{(2)}(t|z_0) = 0$. A parallel reasoning shows that $p_3^{(2)}(t|z_0) = 0$.

To find a suitable reduced ODE for $z^{(2)}(t|z_0)$ start from Eq. (2.9). The right side of Eq. (2.9) is a 6 component vector. The top half of this vector is zero since it is built from the q, p mixed partial derivatives of H which vanish. The Jacobi operator on left of Eq. (2.9) has the matrix form displayed in Eq. (3.10b). It immediately follows that

$$\frac{d}{dt} q^{(2)}(t|z) = \frac{1}{m} p^{(2)}(t|z). \quad (3.14)$$

Inserting this result back into the block matrix form of Eq. (2.9) leads to

$$\begin{aligned}
& m \frac{d^2}{dt^2} q_i^{(2)}(t|z_0) + V_{ij}(q(t|z_0)) q_j^{(2)}(t|z_0) \\
&= -\frac{1}{8} w_{jk}(t|z_0) V_{ijk}(q(t|z_0)) \\
&\quad + \frac{1}{12} w_{jkm}(t|z_0) V_{ijkm}(q(t|z_0)). \quad (3.15)
\end{aligned}$$

Since $q_3^{(2)}(t|z_0) = 0$ the i, j indices on the left side of Eq. (3.15) are restricted to the set $\{1, 2\}$. Thereby Eq. (3.15) is a two-dimensional system of equations for $\{q_1^{(2)}(t|z_0), q_2^{(2)}(t|z_0)\}$. The values of $p^{(2)}(t|z_0)$ are recovered from Eq. (3.14).

In summary, the construction of $\gamma_i^{(2)}$ requires the 92 non-zero components of the tensors ∇g , $\nabla \nabla g$, and $z^{(2)}$. These time dependent functions are obtained as solutions of a linked set of second-order ODE systems with dimensions 10 (∇g), 36 ($\nabla \nabla g$), and 2 ($z^{(2)}$), respectively.

IV. EXPECTATION VALUES

The final stage of calculation is to determine the quantum expectation values $\langle \hat{A}(t) \rangle_\psi$ for physically interesting observables \hat{A} and suitable initial wave functions ψ . We select ψ to be a Gaussian wave function that is sharply peaked in its momentum variable. This allows us to introduce an asymptotic expansion of the momentum portion of the phase-space integral in Eq. (1.6a). As a result the six-dimensional phase space integral is reduced to a three-dimensional one. In addition, by exploiting the tensor structure of an observable, the remaining three-dimensional coordinate integral may be further reduced to a two-dimensional integral.

A. Asymptotic expansion for gaussian wave functions

Observables are most often tensor operators. Let $\hat{T}_{\mu_1 \dots \mu_n}$ be an arbitrary phase space tensor operator having a smooth real valued Weyl symbol $T_{\mu_1 \dots \mu_n}$. For each unit normalized state $\psi \in \mathcal{H}$ with associated Wigner distribution $w_\psi(z)$, the Moyal version of expectation value evolution is [cf. Eq. (1.6a)]

$$\langle \Gamma(t) \hat{T}_{\mu_1 \dots \mu_n} \rangle_\psi = \int_{T^*(\mathbb{R}^3)} dz w_\psi(z) \Gamma_t T_{\mu_1 \dots \mu_n}(z). \quad (4.1)$$

We specialize Eq. (4.1) by choosing ψ to be the displaced Gaussian,

$$\psi(q) = \left(\frac{1}{\pi D^2} \right)^{3/4} \exp \frac{i}{\hbar} (\bar{p} \cdot q) \exp \left[-\frac{1}{2} \left(\frac{q - \bar{q}}{D} \right)^2 \right]. \quad (4.2a)$$

Here the mean position and momentum values are $\langle \hat{q}_j \rangle_\psi = \bar{q}_j$, $\langle \hat{p}_j \rangle_\psi = \bar{p}_j$. The parameter D specifies the half-width, namely, $\langle (\hat{q}_j - \bar{q}_j)^2 \rangle_\psi = \frac{1}{2} D^2$. The Wigner distribution for ψ is

$$\omega_\psi(z) = \left(\frac{2}{\hbar} \right)^3 \exp \left[-\left(\frac{q - \bar{q}}{D} \right)^2 - \left(\frac{D}{\hbar} \right)^2 (p - \bar{p})^2 \right]. \quad (4.2b)$$

Next consider the general features of the p integration in Eq. (4.1). Utilizing the distribution (4.2b) means that this integral has the form

$$H(f; D) \equiv \int d^3 p f(p) \exp[-D^2 \hbar^{-2} (p - \bar{p})^2]. \quad (4.3a)$$

For functions f that are smooth in $p \in \mathbb{R}^3$ this integral has a standard large D asymptotic expansion,

$$H(f; D) = \left(\frac{\pi^{1/2} \hbar}{D} \right)^3 \left[f(\bar{p}) + \frac{1}{4} \left(\frac{\hbar}{D} \right)^2 (\Delta_p f)(\bar{p}) + O\left(\left(\frac{\hbar}{D} \right)^4 \right) \right]. \quad (4.3b)$$

One may verify Eq. (4.3b) by Taylor expanding f about $p = \bar{p}$ and integrating by parts. Due to the symmetry of the Gaussian all the odd order terms vanish. The notation $\Delta_p f$ indicates the Laplacian of f . Observe that the parameters D and \hbar occurring in Eq. (4.3) appear in the combination (\hbar/D) . Thus Eq. (4.3b) is also a small \hbar expansion.

Substituting formula (4.3b) in Eq. (4.1) lets us write

$$\begin{aligned}
\langle \Gamma(t) \hat{T}_{\mu_1 \dots \mu_n} \rangle_\psi &= \frac{1}{(\pi^{1/2} D)^3} \int d^3 q e^{-D^{-2}(q - \bar{q})^2} \tilde{T}_{\mu_1 \dots \mu_n}(q, \bar{p}) \\
&\quad + O\left(\left(\frac{\hbar}{D} \right)^4 \right), \quad (4.4a)
\end{aligned}$$

where the tensor structure is

$$\begin{aligned}
\tilde{T}_{\mu_1 \dots \mu_n}(q, \bar{p}) &= \Gamma_t T_{\mu_1 \dots \mu_n}(q, \bar{p}) \\
&\quad + \frac{1}{4} \left(\frac{\hbar}{D} \right)^2 (\Delta_p \Gamma_t T_{\mu_1 \dots \mu_n}(q, p)) \Big|_{p=\bar{p}}. \quad (4.4b)
\end{aligned}$$

B. Tensor reduction

We choose the phase-space position of ψ so that its mean angular momentum $\bar{q} \times \bar{p}$ lies along the positive e_3 axis. This is achieved if

$$\bar{q} = \bar{b} e_1 + \bar{y} e_2, \quad \bar{p} = \bar{p}_2 e_2, \quad \bar{b} \geq 0, \quad \bar{p}_2 \geq 0. \quad (4.5a)$$

The asymptotic expansion (4.4a) fixes the momentum coordinate to have just one value $p = \bar{p}$. This restricts the allowed class of rigid body rotations (3.8a) to those which preserve the e_2 axis, namely $R_{e_2}(\alpha)$ where $\alpha \in [0, 2\pi)$. The point q is now represented via cylindrical coordinates with α as the angle variable and e_2 as the axis, specifically,

$$\begin{pmatrix} q_1 \\ q_2 \\ q_3 \end{pmatrix} = \begin{pmatrix} \cos \alpha & 0 & \sin \alpha \\ 0 & 1 & 0 \\ -\sin \alpha & 0 & \cos \alpha \end{pmatrix} \begin{pmatrix} b \\ y \\ 0 \end{pmatrix} = \begin{pmatrix} b \cos \alpha \\ y \\ -b \sin \alpha \end{pmatrix}. \quad (4.5b)$$

Here the matrix is the $\{e_i\}$ -basis representation of $R_{e_2}(\alpha)$ and $q_0 = (b, y, 0)$ denotes the $\alpha = 0$ orientation of q .

In the present context the tensor transformation (B7) simplifies to

TABLE I. Potential parameters for He, Ne, Ar.

	He	Ne	Ar
ϵ (cm ⁻¹)	7.103 296	24.812 881	87.018 840
r_{\min} (Å)	2.87	3.131	3.822
σ (Å)	2.56	2.789	3.405
ξ (Å)	1.8	2.1	3.1
a (cm ⁻¹ /Å ⁵)	-4.466 952×10 ⁵	-3.156 232×10 ⁵	-1.583 900×10 ⁴
b (cm ⁻¹ /Å ⁴)	+4.270 465×10 ⁶	+3.519 849×10 ⁶	+2.605 358×10 ⁵
c (cm ⁻¹ /Å ³)	-1.639 362×10 ⁷	-1.576 169×10 ⁷	-1.720 481×10 ⁶
d (cm ⁻¹ /Å ²)	+3.160 429×10 ⁷	+3.544 344×10 ⁷	+5.703 965×10 ⁶
e (cm ⁻¹ /Å)	-3.061 692×10 ⁷	-4.004 876×10 ⁷	-9.498 711×10 ⁶
f (cm ⁻¹)	+1.193 284×10 ⁷	+1.820 423×10 ⁷	+6.359 796×10 ⁶
Mass (amu)	4.0026	20.179	39.948

$$\begin{aligned}\tilde{T}_{\mu_1 \cdots \mu_n}(q, \bar{p}) &= \tilde{T}_{\mu_1 \cdots \mu_n}(R_{e_2} q_0, R_{e_2} \bar{p}) \\ &= \mathcal{R}_{\mu_1 v_1}(\alpha) \cdots \mathcal{R}_{\mu_n v_n}(\alpha) \tilde{T}_{v_1 \cdots v_n}(q_0, \bar{p}).\end{aligned}\quad (4.6a)$$

The α dependence in integral (4.4a) is confined to the factor $(q - \bar{q})^2$ and the matrices $\mathcal{R}_{\mu\nu}(\alpha)$. Denote this generic coupling factor by

$$\begin{aligned}\Omega_{\mu_1 \cdots \mu_n; v_1 \cdots v_n}(b) \\ = \int_0^{2\pi} d\alpha \mathcal{R}_{\mu_1 v_1}(\alpha) \cdots \mathcal{R}_{\mu_n v_n}(\alpha) \exp\left[\frac{2b\bar{b}}{D^2} \cos \alpha\right].\end{aligned}\quad (4.6b)$$

The function Ω is a linear combination of modified Bessel functions I_k with argument $2b\bar{b}/D^2$ and order $k=0, \dots, n$.

The final form of the semiclassical prediction for the observable $\hat{T}_{\mu_1 \cdots \mu_n}$ is obtained by combining Eq. (1.5) together with Eqs. (4.4) and (4.6). Keeping terms to order $O(\hbar^2)$ gives

$$\begin{aligned}\langle \mathbf{\Gamma}(t) \hat{T}_{\mu_1 \cdots \mu_n} \rangle_\psi \\ = \frac{1}{(\pi^{1/2} D)^3} \int_0^\infty b db \int_{-\infty}^\infty dy e^{-D^{-2}[(y-\bar{y})^2 + b^2 + \bar{b}^2]} \\ \times \Omega_{\mu_1 \cdots \mu_n; v_1 \cdots v_n}(b) \left\{ \gamma_t^{(0)} T_{v_1 \cdots v_n}(q_0, \bar{p}) \right. \\ \left. + \frac{1}{2} \hbar^2 \gamma_t^{(2)} T_{v_1 \cdots v_n}(q_0, \bar{p}) \right. \\ \left. + \frac{1}{4} \left(\frac{\hbar}{D} \right)^2 \Delta_p(\gamma_t^{(0)} T_{v_1 \cdots v_n}(q_0, p)) \Big|_{p=\bar{p}} \right\} + O(\hbar^4).\end{aligned}\quad (4.7)$$

The fundamental semiclassical expansion (1.5) resides in the two terms $\gamma_t^{(0)}$ and $\gamma_t^{(2)}$. The additional contribution of order $(\hbar/D)^2$ is not a basic feature of the Moyal semiclassical dynamics but rather is an artifact of our method of approximating the momentum integration. The rate of conver-

gence of the semiclassical expansion is determined by the relative size of the $\gamma_t^{(0)}$ and $\gamma_t^{(2)}$ terms. In Eq. (4.7) all \hbar dependence is explicit. In the following sections for reasons of brevity, the \hbar dependence is implicitly contained in the notation $\tilde{\gamma}_t^{(2)} \equiv \frac{1}{2} \hbar^2 \gamma_t^{(2)}$ and $\tilde{\Delta}_p \equiv \frac{1}{4} (\hbar/D)^2 \Delta_p$. Note that the function Ω and the y, b coordinate part of $\omega_\psi(z)$ are independent of \hbar .

V. NUMERICAL RESULTS

This section presents a number of computational results that serve to profile the convergence and accuracy aspects of the MQM semiclassical expansion. The time dependence of the $\Gamma_t^{(0)}$ and $\Gamma_t^{(2)}$ approximations to expectation values for various observables and initial quantum states is computed. The effect of changing the initial mean wave packet velocity is studied. The relative size of the $\gamma_t^{(0)}$ and $\tilde{\gamma}_t^{(2)}$ terms is determined in the intermediate and long time limit. This ratio is also computed as a function of mass. Finally, we contrast the success of the semiclassical expansion for differing two-atom systems.

The system interaction is given by a modified version of the Lennard-Jones (12-6) potential. The MQM formalism assumes that the Hamiltonian is a differentiable and non-singular function. The Lennard-Jones potential has a strong repulsive core with a r^{-12} singularity at the origin. In this core region we modify the potential so that it is a polynomial in r . It remains strongly repulsive in this core sector. The polynomial coefficients are determined by requiring that the potential have five continuous derivatives, specifically,

$$v(r) = \begin{cases} 4\epsilon[(\sigma/r)^{12} - (\sigma/r)^6], & r \geq \xi \\ ar^5 + br^4 + cr^3 + dr^2 + er + f, & 0 \leq r \leq \xi. \end{cases}\quad (5.1)$$

The parameter ξ is the radial distance where the smooth inner core region is fitted onto the Lennard-Jones form. The potential energy at this match point is at least three times greater than the total mean energy of the system for the calculations displayed in this section. The constants in the formula (5.1) are found in Table I. The parameter values ϵ and σ for He, Ne, and Ar are found in Refs. [37-39], respectively.

The general effect of the strong repulsive core is to make the quantum wave function exponentially small within the core volume. For this reason one expects that the smooth

TABLE II. Linear observables for He at $c=450$ m/s.

Time (10^{-10} s)	$\langle \gamma_t^{(0)}(q_1) \rangle$	$\langle \tilde{\gamma}_t^{(2)}(q_1) \rangle$	$\langle \tilde{\Delta}_p \gamma_t^{(0)}(q_1) \rangle$ (\AA)	$\langle \gamma_t^{(0)}(q_2) \rangle$	$\langle \tilde{\gamma}_t^{(2)}(q_2) \rangle$	$\langle \tilde{\Delta}_p \gamma_t^{(0)}(q_2) \rangle$
0.0000	2.000	0	0	$-1.400 \times 10^{+2}$	0	0
0.2800	2.000	2.510×10^{-5}	2.575×10^{-5}	$-1.403 \times 10^{+1}$	7.446×10^{-3}	-5.790×10^{-4}
0.3111	1.999	1.477×10^{-4}	1.669×10^{-4}	-1.229×10^{-1}	3.851×10^{-2}	2.816×10^{-3}
0.3422	1.997	4.599×10^{-4}	5.357×10^{-4}	$1.367 \times 10^{+1}$	1.120×10^{-1}	1.558×10^{-2}
0.3533	1.997	6.142×10^{-4}	7.150×10^{-4}	$1.858 \times 10^{+1}$	1.474×10^{-1}	2.191×10^{-2}
0.3667	1.996	8.180×10^{-4}	9.476×10^{-4}	$2.446 \times 10^{+1}$	1.937×10^{-1}	2.992×10^{-2}
0.4889	1.985	2.867×10^{-3}	3.179×10^{-3}	$7.830 \times 10^{+1}$	6.551×10^{-1}	1.014×10^{-1}
0.4978	1.984	3.017×10^{-3}	3.341×10^{-3}	$8.221 \times 10^{+1}$	6.888×10^{-1}	1.065×10^{-1}
Time (10^{-10} s)	$\langle \gamma_t^{(0)}(p_1) \rangle$	$\langle \tilde{\gamma}_t^{(2)}(p_1) \rangle$	$\langle \tilde{\Delta}_p \gamma_t^{(0)}(p_1) \rangle$ (amu m/s)	$\langle \gamma_t^{(0)}(p_2) \rangle$	$\langle \tilde{\gamma}_t^{(2)}(p_2) \rangle$	$\langle \tilde{\Delta}_p \gamma_t^{(0)}(p_2) \rangle$
0.0000	0	0	0	90.058	0	0
0.2800	-2.322×10^{-2}	3.474×10^{-3}	3.795×10^{-3}	89.740	0.948	0.022
0.3111	-7.733×10^{-2}	1.351×10^{-2}	1.592×10^{-2}	89.092	3.292	0.497
0.3422	-1.382×10^{-1}	2.614×10^{-2}	3.063×10^{-2}	88.452	6.025	1.086
0.3533	-1.524×10^{-1}	2.926×10^{-2}	3.376×10^{-2}	88.317	6.677	1.180
0.3667	-1.631×10^{-1}	3.168×10^{-2}	3.579×10^{-2}	88.220	7.176	1.214
0.4889	-1.721×10^{-1}	3.378×10^{-2}	3.654×10^{-2}	88.144	7.602	1.157
0.4978	-1.721×10^{-1}	3.378×10^{-2}	3.654×10^{-2}	88.144	7.602	1.157

modification of the potential within the core region will have no noticeable effect on observable quantities. We have checked this assumption by changing the He matching radius from $\xi=1.8$ \AA to $\xi=1.7$ \AA . This reduction of ξ increases the energy of $v(\xi)$ from 1710.8 cm^{-1} to 3531.6 cm^{-1} . To the level of accuracy displayed in Tables II–V none of the reported values change.

The atomic systems studied here are identical pairs of helium, neon, and argon atoms. These systems vary by a factor of 10 in mass, and as Fig. 1 shows have attractive potential well depths that also vary by approximately a factor of 10.

The preevolution state of the system will always be the displaced Gaussian Wigner distribution $w_\psi(z)$. This function (4.2b) is determined by four parameters, \bar{b} , \bar{y} , D , and \bar{p}_2 . The first three of these will have a fixed set of values chosen to represent an initial state consistent with scattering boundary conditions. These fixed values are $\bar{b}=2$ \AA , $\bar{y}=-140$ \AA , and $D=20$ \AA . These values ensure at time $t=0$

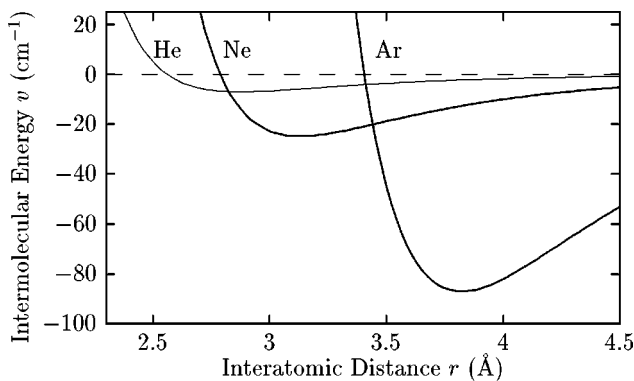


FIG. 1. Lennard-Jones potentials for He, Ne, and Ar.

that the potential energy of the system is negligible (1 part in 10^{10}) relative to the kinetic energy. The large value of the half width D causes the asymptotic momentum expansion factor $\tilde{\Delta}_p \gamma_t^{(0)}$ to be comparable to the $\tilde{\gamma}_t^{(2)}$ term. The initial closing velocity $c=\bar{p}_2/m$ will take on a range of values.

In order to obtain accurate values for the two dimensional integral in Eq. (4.7), which determines quantum averages, a large number of integration points is required. A typical expectation value reported in the tables uses about 32 000 phase space points. Each point is an initial value of a trajectory. Along each trajectory we solve the ODE system described in Sec. III for the 92 time dependent functions needed for the calculation of $\gamma_t^{(2)}$.

A. General features of the numerical solutions

Let us first examine the He atom system with initial velocity $v=450$ m/s. The pair of plots in Fig. 2 contrasts the $\Gamma_t^{(0)}z=q(t|z)$ (classical) and $\Gamma_t^{(2)}z$ (quantum) trajectories projected onto the q_1 - q_2 (or b - y) plane. For large impact parameter $b>4$ \AA there is little difference in the spray of these two sets of trajectories, but for small b (where the potential is large) they are often strikingly different. Both sets of trajectories stay outside the smooth core region $r<\xi$, which is indicated by the closed curve about $r=0$. At $b=3.06$ \AA the classical trajectory has the same initial and final impact parameter. This defines classical glory scattering. When $b=3.62$ \AA the classical trajectory undergoes rainbow scattering and has its maximum angular displacement with respect to the y axis. It is interesting to note that, once the impact parameter is outside the region between glory scattering and rainbow scattering, the large time behavior of the classical and quantum trajectories is very similar.

A useful quantity in describing the system evolution is the mean closest approach time, t_c . At this time the wave packet is centered above the origin and potential dependent effects are strongest. Technically, we define the time t_c to be the time for which $\langle \Gamma_t^{(0)} q^2 \rangle_\psi$ has its minimum.

Table II records the expectation values of all the nonzero linear canonical operators (q_1, q_2, p_1, p_2) for eight different times. In the second, third, and fourth columns, the displayed averages correspond to the $\gamma_t^{(0)}$, $\tilde{\gamma}_t^{(2)}$, and $\tilde{\Delta}_p \gamma_t^{(0)}$ contributions to $\langle \Gamma(t) q_1 \rangle_\psi$, respectively. The mean closest approach occurs at $t_c = 0.3111$. At the final time 0.4978, the system is in a postscattering configuration where the potential-energy effects are negligible. For linear observables, $\gamma_t^{(2)}$ is determined solely by the quantum trajectories; the $w_{\alpha\beta}$ and $w_{\alpha\beta\gamma}$ portions of $\gamma_t^{(2)}$ vanish in this case. The units for momentum are amu m/s. The operators \hat{q}_3 and \hat{p}_3 are not listed in Table II. The planar motion invariance causes these expectation values to be zero.

As the collision process takes place the wave function will lose its initial coherent state (Gaussian) character. Correspondingly, the product of uncertainties $\Delta p_j \Delta q_j$ appearing in the Heisenberg uncertainty relation $\Delta p_j \Delta q_j \geq \frac{1}{2} \hbar$ will grow in time. Table III displays this changing uncertainty computed to order $O(\hbar^2)$ for the canonical pairs (q_j, p_j) , $j = 1, 2$. The effect of the collision processes produces a substantial deviation from the initial coherent state. Cylindrical symmetry about the y axis implies that the uncertainty $\Delta q_3 \Delta p_3$ is the same as $\Delta q_1 \Delta p_1$.

In Table IV the same system and initial state are employed as in Tables II and III. These results display the expectation values for the potential v and all the scalar quadratic observables $(q^2, p^2, q \cdot p)$. The apparent trend that holds for the eight observables shown in Tables II and IV is that the leading semiclassical term $\gamma_t^{(0)}$ significantly dominates the second order $\tilde{\gamma}_t^{(2)}$ corrections, typically by a factor of 10 or more. The potential is a particularly sensitive test observable since it depends on all parts of the $\gamma_t^{(2)}$ operator. The quadratic observables have no contribution from the $w_{\alpha\beta\gamma}$ terms. At closest approach time 0.3111 the $O(\hbar^2)$ correction for the potential is 8.5% of the leading $\gamma_t^{(0)}(v)$ term. Of the eight observables examined here the largest relative corrections occur for p_1 . However, this observable is non-typical in that its initial mean value is zero and its later time

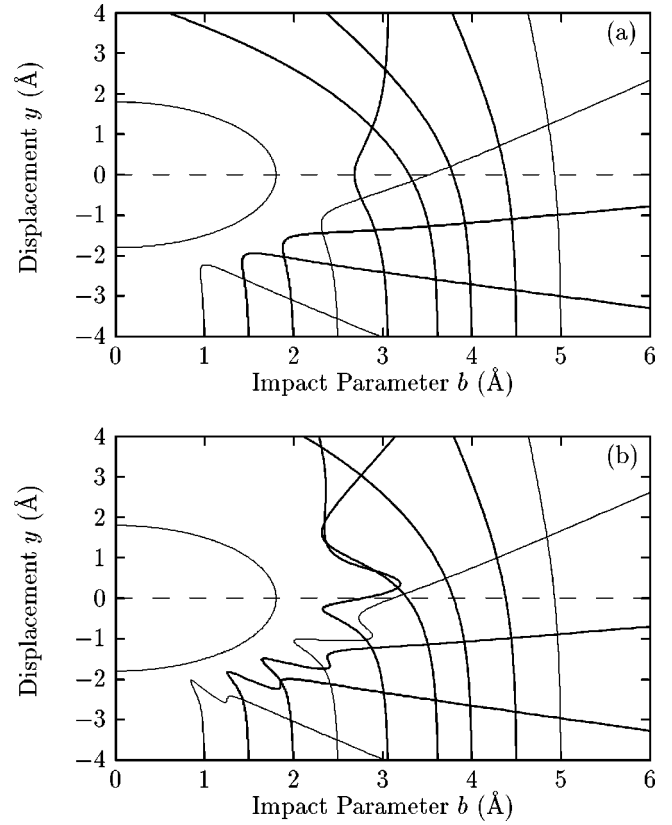


FIG. 2. (a) Classical and (b) quantum trajectories for He at $c = 450$ m/s.

$\gamma_t^{(0)}$ values remain close to zero. Throughout, corrections arising from the asymptotic momentum expansion $\tilde{\Delta}_p \gamma_t^{(0)}$ are of the same order of magnitude as those for $\tilde{\gamma}_t^{(2)}$.

B. Convergence and stability of classical flow

The next set of calculations, shown in Table V, explores the role of the initial wave-packet energy and how it effects the convergence of the semiclassical expansion. The system remains He and as c varies (and hence the incident energy) the parameters \bar{b}, \bar{y}, D are kept fixed to the values used above. The times in the list shown correspond to the closest approach time. The general outcome is that the relative size

TABLE III. Heisenberg uncertainty.

Time	Δq_1	Δp_1	$\frac{2}{\hbar} \Delta q_1 \Delta p_1^a$	Δq_2	Δp_2	$\frac{2}{\hbar} \Delta q_2 \Delta p_2^a$
(10^{-10} s)	(Å)	(amu m/s)		(Å)	(amu m/s)	
0.0000	14.1421	22.453	1.0000	14.1421	22.453	1.0000
0.2800	14.4893	36.219	1.6527	14.4658	60.518	2.7570
0.3111	14.5801	47.999	2.2039	14.5521	92.936	4.2590
0.3422	14.6997	53.105	2.4584	14.7831	112.59	5.2419
0.3533	14.7514	53.595	2.4898	14.9192	115.94	5.4474
0.3667	14.8205	53.803	2.5112	15.1219	118.21	5.6292
0.4889	15.8169	53.888	2.6842	18.5840	119.91	7.0178
0.4978	15.9135	53.888	2.7006	18.9222	119.91	7.1455

^a $\hbar = 1.054\,572\,7 \times 10^{-34}$ J·s = 635.078 07 Å amu m/s.

TABLE IV. Potential and quadratic observables for He.

Time (10^{-10} s)	$\langle \gamma_i^{(0)}(v) \rangle$	$\langle \tilde{\gamma}_i^{(2)}(v) \rangle$ (cm^{-1})	$\langle \tilde{\Delta}_p \gamma_i^{(0)}(v) \rangle$	$\langle \gamma_i^{(0)}(q \cdot p) \rangle$	$\langle \tilde{\gamma}_i^{(2)}(q \cdot p) \rangle$ ($\text{amu } \text{Å}^2/10^{-10} \text{ s}$)	$\langle \tilde{\Delta}_p \gamma_i^{(0)}(q \cdot p) \rangle$
0.0000	-1.251×10^{-9}	0	0	$-1.261 \times 10^{+5}$	0	0
0.2800	-1.862×10^{-2}	1.177×10^{-3}	9.618×10^{-4}	$-1.261 \times 10^{+4}$	-0.223	211.50
0.3111	-2.955×10^{-2}	2.517×10^{-3}	2.628×10^{-3}	$1.384 \times 10^{+1}$	0.396	234.35
0.3422	-1.813×10^{-2}	1.983×10^{-3}	1.301×10^{-3}	$1.263 \times 10^{+4}$	2.079	257.32
0.3533	-1.210×10^{-2}	1.433×10^{-3}	5.170×10^{-4}	$1.713 \times 10^{+4}$	2.628	265.69
0.3667	-6.349×10^{-3}	8.219×10^{-4}	-4.888×10^{-5}	$2.254 \times 10^{+4}$	3.103	275.74
0.4889	-6.307×10^{-8}	3.281×10^{-9}	-3.621×10^{-8}	$7.206 \times 10^{+4}$	3.582	368.21
0.4978	-4.058×10^{-8}	9.261×10^{-11}	-5.077×10^{-9}	$7.566 \times 10^{+4}$	3.582	374.91
Time (10^{-10} s)	$\langle \gamma_i^{(0)}(q^2) \rangle$	$\langle \tilde{\gamma}_i^{(2)}(q^2) \rangle$ (Å^2)	$\langle \tilde{\Delta}_p \gamma_i^{(0)}(q^2) \rangle$	$\langle \gamma_i^{(0)}(p^2) \rangle$	$\langle \tilde{\gamma}_i^{(2)}(p^2) \rangle$ [(amu m/s^2) ²]	$\langle \tilde{\Delta}_p \gamma_i^{(0)}(p^2) \rangle$
0.0000	$2.020 \times 10^{+4}$	0	0	$8.111 \times 10^{+5}$	0	1512.5
0.2800	$8.001 \times 10^{+2}$	-6.553×10^{-3}	$2.961 \times 10^{+1}$	$8.119 \times 10^{+5}$	-56.370	1466.4
0.3111	$6.044 \times 10^{+2}$	-7.211×10^{-3}	$3.654 \times 10^{+1}$	$8.125 \times 10^{+5}$	-120.52	1386.6
0.3422	$8.009 \times 10^{+2}$	3.016×10^{-2}	$4.418 \times 10^{+1}$	$8.119 \times 10^{+5}$	-94.962	1450.2
0.3533	$9.661 \times 10^{+2}$	5.641×10^{-2}	$4.709 \times 10^{+1}$	$8.116 \times 10^{+5}$	-68.615	1487.7
0.3667	$1.230 \times 10^{+3}$	9.483×10^{-2}	$5.069 \times 10^{+1}$	$8.114 \times 10^{+5}$	-39.343	1514.8
0.4889	$7.008 \times 10^{+3}$	5.254×10^{-1}	$9.002 \times 10^{+1}$	$8.111 \times 10^{+5}$	0.014	1512.5
0.4978	$7.664 \times 10^{+3}$	5.572×10^{-1}	$9.332 \times 10^{+1}$	$8.111 \times 10^{+5}$	0.014	1512.5

of the $\tilde{\gamma}_i^{(2)}$ vis-à-vis the $\gamma_i^{(0)}$ contributions systematically decrease with increasing energy. At velocities below 290 m/s $\tilde{\gamma}_i^{(2)}$ numerically diverges at finite time displacement and the approximation fails.

It is important to isolate which features of the dynamics are responsible for this convergence behavior. Simply put, the stability of the classical motion controls whether or not one obtains accurate approximation valid for times exceeding the duration of the scattering process.

To begin we identify the unstable classical trajectories present in this problem. All these motions are associated with an unstable equilibrium point. In spherical coordinates the radial pair of Hamilton's equations are

$$\dot{r} = p_r/m, \quad \dot{p}_r = -v_e'(r), \quad (5.2)$$

where $v_e(r)$ is the effective potential $v(r) + L^2/(2mr^2)$. A fixed point occurs if the right-hand sides of Eq. (5.2) vanish. This point is stable if $v_e''(r) > 0$ and unstable if $v_e''(r) < 0$. For given L denote by r_0 the radial value of the unstable fixed point.

Consider the family of circular orbits. Whenever initial data satisfies $v_e'(r) = 0$ and $p_r = 0$ circular motion results. For $v_e''(r) > 0$ the orbit is the stable minimum energy state consistent with L . On the other hand, when $v_e''(r_0) < 0$ then an unstable orbit arises. As one increases the energy the radii of the stable and unstable orbits approach each other and coalesce when $v_e''(r) = 0$. This happens at the critical energy $E_c = \frac{4}{3}\epsilon$, cf. (5.1). The unstable fixed points have a finite range of energies, $0 < E < \frac{4}{3}\epsilon$.

A related class of unstable motions are those that con-

TABLE V. Velocity dependence and semiclassical convergence for He.

Velocity (m/s)	Time (10^{-10} s)	$\langle \gamma_i^{(0)}(q_1) \rangle$ (Å)	$\frac{\langle \tilde{\gamma}_i^{(2)}(q_1) \rangle}{\langle \gamma_i^{(0)}(q_1) \rangle}$	$\langle \gamma_i^{(0)}(q \cdot p) \rangle$ ($\text{amu } \text{Å}^2/10^{-10} \text{ s}$)	$\frac{\langle \tilde{\gamma}_i^{(2)}(q \cdot p) \rangle}{\langle \gamma_i^{(0)}(q \cdot p) \rangle}$	$\langle \gamma_i^{(0)}(q_2^2) \rangle$ (Å^2)	$\frac{\langle \tilde{\gamma}_i^{(2)}(q_2^2) \rangle}{\langle \gamma_i^{(0)}(q_2^2) \rangle}$
280	0.5000	1.998	-2.117×10^{-3}	3.0603	1.0×10^{12}	197.523	1.0×10^7
290	0.4828	1.998	-2.896×10^{-3}	3.6331	-2.378	197.575	-5.512×10^{-3}
300	0.4667	1.998	-2.453×10^{-3}	4.2491	-1.415	197.609	-3.256×10^{-2}
350	0.4000	1.998	-6.177×10^{-4}	7.5245	-0.1781	197.858	-5.766×10^{-3}
400	0.3500	1.999	-1.588×10^{-4}	10.770	-0.009 70	198.201	5.218×10^{-3}
450	0.3111	1.999	7.388×10^{-5}	13.840	0.028 61	198.475	5.703×10^{-3}
500	0.2800	1.999	1.128×10^{-4}	16.724	0.037 57	198.666	4.437×10^{-3}
550	0.2545	2.000	1.152×10^{-4}	19.427	0.038 08	198.796	3.213×10^{-3}
600	0.2333	2.000	1.062×10^{-4}	21.963	0.035 94	198.885	2.295×10^{-3}
650	0.2154	2.000	9.442×10^{-5}	24.356	0.033 07	198.948	1.646×10^{-3}

verge to the fixed point as $t \rightarrow \infty$. Among these are the trapped scattering states. These states have an initial radial position $r > r_0$ and an energy equal to the $v_e(r_0)$. As $t \rightarrow \infty$ then $r(t) \rightarrow r_0$ and $p_r(t) \rightarrow 0$.

The stability aspect of a periodic flow is determined by its Lyapunov [40] exponents. For any point z_c on a circular orbit, a simple calculation in spherical coordinates shows $J\nabla\nabla H(g(t|z_c))$ to be a time independent matrix. Thus the Jacobi field has the exponential representation

$$\nabla g(t|z_c) = e^{tJ\nabla\nabla H(z_c)}. \quad (5.3)$$

It is readily found that $J\nabla\nabla H(z_c)$ has the eigenvalue, $\lambda = \sqrt{-v_e''(r(z_c))/m}$. This is positive if $r(z_c) = r_0$ and verifies that the associated state is an unstable periodic orbit. A similar analysis applies to the trapped scattering trajectory. As $t \rightarrow \infty$ the matrix $J\nabla\nabla H(g(t|z))$ converges to $J\nabla\nabla H(z_c)$. Again one has exponential growth of the Jacobi field.

Away from the family of unstable motions, complete integrability of the system guarantees that there is stable classical flow. The three constants of motion are $H(z)$, $L^2(z)$, and $L_3(z)$. These functions are all in involution, and independent in $\mathbb{R}_q^3 \times \mathbb{R}_p^3$ except on a set of measure zero that includes all unstable orbits. For bounded motion with $v_e'(r) \neq 0$ one may show that the Jacobi field written in action-angle variables is a linear function of time. For scattering trajectories with $v_e'(r) \neq 0$ a similar result holds. The numerical values of the Jacobi fields reflect exactly this predicted behavior.

With these considerations in mind let us return to the interpretation of the numerical results in Table V. The velocity c_c corresponding to the critical energy E_c is 260 m/s. For incident velocities that are 20% greater than v_c we have uniformly good convergence of the two-term semiclassical expansion at post collision times. However, for velocities sufficiently near c_c some of the trajectories used in the expectation value formula (4.7) closely approach the unstable trapped scattering trajectory. In these circumstances the trajectory will loop around the origin a finite number of times before moving away from the potential region. When this happens (cf. $c = 280$ case in Table V) the Jacobi fields grow rapidly; at a finite time displacement $\tilde{\gamma}_t^{(2)}$ has unbounded numerical values.

C. Long-time behavior

An aspect of semiclassical approximation that has received much attention in the literature is its long time behavior. For dynamical systems that have regions of instability (positive Lyapunov exponent λ) it is expected [41–44,34] that the approximation $\langle \Gamma_t A \rangle_\psi \approx \langle \Gamma_t^{(N)} A \rangle_\psi$ can be accurate only for a finite time interval $[0, T]$ of the order $T \approx \text{const} \cdot \lambda^{-1} \ln(\hbar^{-1})$. For this reason it is of interest to study the long time regime for our expansion (4.7).

In order to profile numerically the typical $t \rightarrow \infty$ structure we examine the expectation value $\langle \Gamma_t q^2 \rangle_\psi$. This quantity has quadratic growth for large t and is sensitive to both wave packet transport and spreading. For mean velocities c greater than the unstable case c_c it is found that the fractional correction $\langle \tilde{\gamma}_t^{(2)}(q^2) \rangle / \langle \gamma_t^{(0)}(q^2) \rangle$ becomes constant as $t \rightarrow \infty$. Figure 3 shows this result for $c = 450$ m/s.

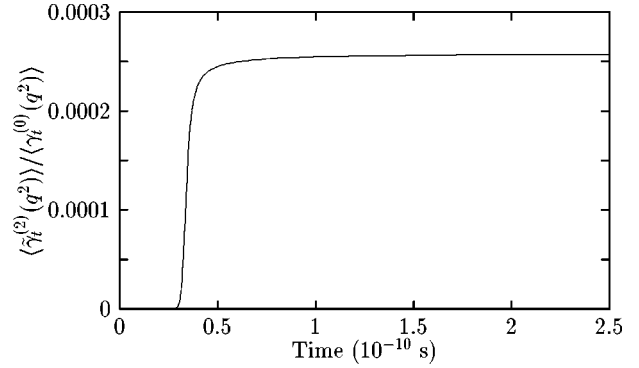


FIG. 3. Time dependence of relative size of correction.

Two qualifying remarks need to be made about the implications of the long time accuracy displayed in Fig. 3. The first is that the set of scattering trajectories that enter the $c = 450$ m/s expectation value calculation are not close to the unstable motions, so one would not expect the $\ln(\hbar^{-1})$ time restriction to apply. Second, it should be emphasized that our calculations only report the values of $\langle \gamma_t^{(n)} A \rangle_\psi$, $n = 0, 2$ and not the difference $\langle \Gamma_t A \rangle_\psi - \langle \Gamma_t^{(N)} A \rangle_\psi$. Although our calculations do not directly show the $\ln(\hbar^{-1})$ time restriction, its underlying cause—unstable classical flow—does play a controlling role in determining the range of initial energies for which there is an accurate two term semiclassical approximation.

D. Mass and system dependence

As the mass of the atom increases, the system dynamics will become more classical. We measure this effect by calculating the ratio of $\langle \tilde{\gamma}_t^{(2)}(A) \rangle / \langle \gamma_t^{(0)}(A) \rangle$ for the observable $A = q \cdot p$, while artificially increasing the mass from $0.5m_{He}$ to $10m_{He}$. Figure 4 shows that this ratio varies basically as m^{-2} for large m .

Our last calculation compares the semiclassical convergence as one varies the atomic system among He, Ne, and Ar. These calculations have common initial velocity $c = 450$ m/s and display the $\langle \gamma_t^{(0)}(A) \rangle$ and the $\langle \tilde{\gamma}_t^{(2)}(A) \rangle / \langle \gamma_t^{(0)}(A) \rangle$ ratio at time t_c of closest approach as well as at t_f the postcollision time. The observables A are p_2 , $q \cdot p$, and q_1^2 . Increased mass makes the $\tilde{\gamma}_t^{(2)}$ effects smaller while increased potential makes it larger. Table VI clearly shows that

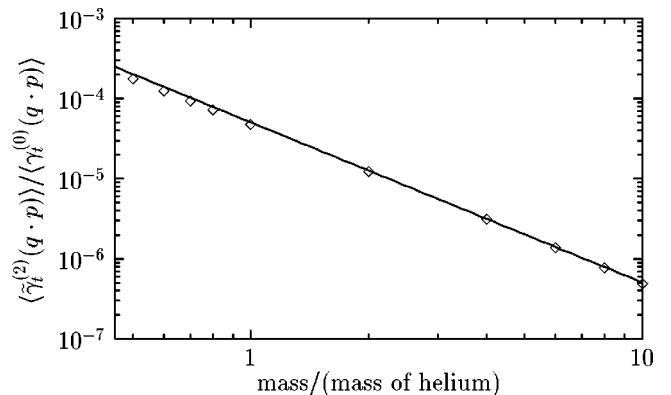


FIG. 4. Mass dependence of $\langle \tilde{\gamma}_t^{(2)}(q \cdot p) \rangle / \langle \gamma_t^{(0)}(q \cdot p) \rangle$.

TABLE VI. Atomic system comparison.

	$\langle \gamma_i^{(0)}(p_2) \rangle$	$\frac{\langle \tilde{\gamma}_i^{(2)}(p_2) \rangle}{\langle \gamma_i^{(0)}(p_2) \rangle}$	$\langle \gamma_i^{(0)}(q \cdot p) \rangle$	$\frac{\langle \tilde{\gamma}_i^{(2)}(q \cdot p) \rangle}{\langle \gamma_i^{(0)}(q \cdot p) \rangle}$	$\langle \gamma_i^{(0)}(q_1^2) \rangle$	$\frac{\langle \tilde{\gamma}_i^{(2)}(q_1^2) \rangle}{\langle \gamma_i^{(0)}(q_1^2) \rangle}$
	(amu m/s)		(amu $\text{\AA}^2/10^{-10}$ s)		(\AA^2)	
$t_c = 0.3111 \times 10^{-10}$ s						
Helium	89.092	3.695×10^{-2}	$1.384 \times 10^{+1}$	2.861×10^{-2}	204.958	-2.780×10^{-3}
Neon	448.96	1.056×10^{-4}	$1.054 \times 10^{+2}$	1.589×10^{-3}	204.991	-9.185×10^{-5}
Argon	880.21	3.913×10^{-5}	$3.492 \times 10^{+2}$	-2.270×10^{-4}	205.865	-2.159×10^{-5}
$t_f = 0.4978 \times 10^{-10}$ s						
Helium	88.144	8.625×10^{-3}	$7.566 \times 10^{+4}$	4.734×10^{-5}	275.503	-1.646×10^{-1}
Neon	444.29	2.384×10^{-4}	$3.816 \times 10^{+5}$	2.067×10^{-6}	272.374	-5.629×10^{-3}
Argon	861.31	1.027×10^{-4}	$7.554 \times 10^{+5}$	5.940×10^{-7}	346.050	-9.706×10^{-4}

the mass effect dominates this balance.

VI. DISCUSSION AND CONCLUSIONS

The MQM semiclassical expansion approximates the Heisenberg-Weyl evolution operator Γ_t by $\Gamma_t^{(N)}$. The semiclassical evolution $\Gamma_t^{(N)}$ is given by a power series in \hbar with operator valued coefficients $\gamma_i^{(n)}$ that map the Weyl symbol of an observable onto its related dynamical value. The leading $\gamma_i^{(0)}$ term is determined by classical flow in phase space. The connected graph approach of Osborn and Molzahn [30] shows that the higher-order coefficient operators $\gamma_i^{(n)}$, $n \geq 1$, are given by a universal function of the Poisson bracket operators B_{ij} and finite-order phase-space gradients. Quantum expectation values are phase-space integrals. The approximate evolution $\Gamma_t^{(N)}$ preserves wave-function norm. For Weyl quantized systems, $\gamma_i^{(2)}$ is the first nonzero correction beyond the leading term $\gamma_i^{(0)}$. The operators $\gamma_i^{(n)}$ are obtained computationally from finite systems of ODE's.

These features show that this semiclassical approximation is structurally very different from the better known WKB [45,46,35] approximation. In the MQM $\Gamma_t^{(N)}$ expansion there are no caustics, no multiple two-point boundary condition trajectories, and no essential singularities as $\hbar \downarrow 0$. For these reasons the MQM semiclassical expansion is more readily applied to physical problems than is the WKB expansion.

A remaining question that is important to resolve is: ‘‘What is the small parameter responsible for making $\frac{1}{2}\hbar^2\gamma_i^{(2)}$ a small correction to $\gamma_i^{(0)}$?’’ The mathematical procedures used in the derivation of expansion (1.5) and what one does in the practical applications (as reported in Sec. V) are near opposites. In obtaining Eq. (1.5) analytically, it is assumed that \hbar is small and one can scale this parameter to zero. In this fashion, the formulas for $\gamma_i^{(n)}$ are derived and the error bound estimate (2.3b) acquires significance. However, in a numerical modeling of a realistic system, the value \hbar is set to its physical value and cannot vary. So, what is the scaling structure that makes the semiclassical expansion valid? The following argument gives a simple guide that shows when the higher-order $O(\hbar^2)$ corrections cease to be significant. Observe that the derivative structure of $\gamma_i^{(2)}$ [cf. Eq. (2.11)] is similar to the terms appearing in a Taylor series expansion of a symbol A about the point $g(t|z)$. Let δz

be the least phase space displacement such that

$$|\delta z_\alpha| \geq \frac{\hbar^2}{2} |z_\alpha^{(2)}(t|z)|, \quad |\delta z_\alpha \delta z_\beta| \geq \frac{\hbar^2}{8} |w_{\alpha\beta}(t|z)|,$$

$$|\delta z_\alpha \delta z_\beta \delta z_\gamma| \geq \frac{\hbar^2}{4} |w_{\alpha\beta\gamma}(t|z)|.$$

A Taylor series expansion of $A(g(t|z) + \delta z)$ in the variable δz has $\gamma_i^{(0)}A(z)$ as its first term. The next three derivative terms are all individually larger than the corresponding derivatives in formula (2.11) for $\frac{1}{2}\hbar^2\gamma_i^{(2)}A(z)$. The conclusion is that whenever $A(g(t|z) + \delta z)$ is accurately approximated by its two term Taylor series expansion in δz (roughly, when A is slowly varying with respect to the phase-space distance $|\delta z|$), then the $O(\hbar^0)$ semiclassical approximation is valid.

The simplicity of the MQM semiclassical expansion has meant that we have been able to calculate both of the semiclassical evolution operators $\Gamma_t^{(0)}$ and $\Gamma_t^{(2)}$; and further, to make a detailed comparison of their predictions for expectation values. Specifically, the Lennard-Jones potential (5.1) provides a consistent description of the helium-helium atom system for collision energies that range from the inelastic threshold down to zero. For helium the first excited state occurs at $E = 159\,850 \text{ cm}^{-1}$ and the corresponding incident velocity for the threshold is $c = 43\,700 \text{ m/s}$. Assuming Gaussian Wigner distributions for the initial state, the Moyal semiclassical expansion (4.7) is valid from 350 m/s to 43 700 m/s. Similar remarks apply to the neon and argon systems. Collectively, our numerical results establish the computational feasibility and accuracy of the MQM semiclassical expansion for a wide range of initial states in the helium, neon, and argon systems.

ACKNOWLEDGMENTS

The authors would like to thank our colleagues F. H. Molzahn, M. V. Karasev, and S. F. Fulling for critically reading the manuscript and suggesting a number of improvements. We are especially thankful for the assistance of M. F. Kondrat'eva who, in addition to help with the manuscript, checked many of the equations in the text. This research was supported in part by grants to T.A.O. and G.C.T. from the

Natural Sciences and Engineering Research Council of Canada. B.R.McQ. gratefully acknowledges support from the NSERC. Furthermore, the support from the Office of Research Administration and the Faculty of Science at the University of Manitoba assisted in the purchase of new computational facilities that were essential for this project.

APPENDIX A: ASPECTS OF WEYL SYMBOL CALCULUS

The Moyal formalism requires several basic features of the Weyl symbol calculus. These identities and expansions are collected together in this appendix.

The linear operators on Hilbert space form a Lie algebra the bracket of which is the commutator. The Wigner transform from operators to symbols is a homomorphism that preserves the bracket (commutator) operation. In order that the product of Hilbert space operators correspond to a ‘product’ of symbols, a noncommutative extension of scalar multiplication is required. This is the $*$ product. Let \hat{X}, \hat{Y} be two operators with symbols X, Y . The $*$ operation on this symbol pair is defined as

$$X*Y \equiv \sigma(\hat{X}\hat{Y}). \tag{A1}$$

A well-known integral formula [6] for this product is

$$X*Y(z) = (\pi\hbar)^{-6} \int \int d\zeta d\zeta' X(z+\zeta)Y(z+\zeta') \exp\left[\frac{2i}{\hbar}\zeta \cdot J\zeta'\right]. \tag{A2}$$

Here J is the Poisson matrix

$$J = \begin{bmatrix} 0 & \delta \\ -\delta & 0 \end{bmatrix}. \tag{A3}$$

The $*$ operation is a noncommutative associative product of symbols.

The Moyal bracket is the σ image of the quantum commutator,

$$\{X, Y\}_M \equiv \sigma\left(\frac{1}{i\hbar}[X, Y]\right) = \frac{1}{i\hbar}(X*Y - Y*X). \tag{A4}$$

Like the commutator, the Moyal bracket is bilinear, skew, and obeys the Jacobi identity.

Frequently the symbols of operators are smooth differentiable functions on phase space. In this case the $*$ product and the Moyal bracket admit derivative based representations. Let B_{12} denote an extended Poisson bracket operator $B_{12} = \nabla_1 \cdot J \nabla_2$. Acting on the tuple $\langle X, Y \rangle$, the action of B_{12}^n is (after diagonal evaluation $z' = z$)

$$B_{12}^n \langle X, Y \rangle(z) = X_{,\mu_1 \dots \mu_n}(z) J_{\mu_1 \nu_1} \dots J_{\mu_n \nu_n} Y_{;\nu_1 \dots \nu_n}(z). \tag{A5}$$

If $n = 1$ then Eq. (A5) reproduces the Poisson bracket

$$B_{12} \langle X, Y \rangle(z) = \{X, Y\}(z) \equiv \nabla X(z) \cdot J \nabla Y(z). \tag{A6}$$

In terms of B_{12} the $*$ product has the Groenewold representation [2]

$$X*Y(z) = \exp\left[\frac{i\hbar}{2} B_{12}\right] \langle X, Y \rangle(z). \tag{A7}$$

This formal expression for $X*Y$ follows easily [30] from (A2).

It is important to have small \hbar asymptotic expansions of the Moyal bracket. Such an expansion is obtained on combining (A7) and (A4), specifically,

$$\begin{aligned} \{X, Y\}_M(z) &= \frac{2}{\hbar} \sin\left(\frac{\hbar}{2} B_{12}\right) \langle X, Y \rangle(z) \\ &= \{X, Y\}(z) - \left(\frac{\hbar}{2}\right)^2 \frac{1}{3!} B_{12}^3 \langle X, Y \rangle(z) + \dots \end{aligned} \tag{A8a}$$

$$\tag{A8b}$$

The asymptotic expansion (A8b) shows how the Moyal bracket modifies the classical Poisson bracket via the addition of an ascending series of higher-order \hbar correction terms.

In the density matrix formalism, quantum expectation values are determined in terms of traces of Hilbert space operators. Fortunately the link between the trace evaluation and the symbol is straightforward. We require two identities:

$$\text{Tr } \hat{X} = \int dq \langle q | \hat{X} | q \rangle = \hbar^{-3} \int dz X(z), \tag{A9a}$$

$$\text{Tr } \hat{X}\hat{Y} = \hbar^{-3} \int dz X(z)Y(z). \tag{A9b}$$

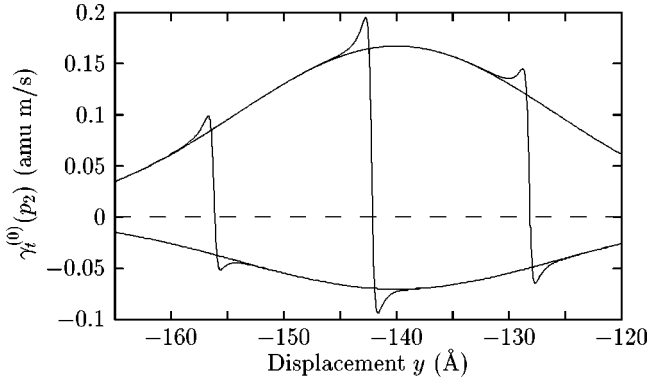
Utilizing Eq. (A9a) to obtain Eq. (A9b) initially leads to an integrand $X*Y(z)$. However, using the representation (A7) coupled with an integration by parts argument shows that all the higher-order B_{12}^n terms vanish leaving the result displayed in Eq. (A9b).

The operator valued semiclassical expansion (1.5) with the accompanying representation for $\gamma_t^{(2)}$ is the basis of all the subsequent numerical calculations. It is useful to tie these results into the mathematical literature on Weyl symbol calculus and to obtain an independent check on formula (2.11). An \hbar expansion having similar content to Eq. (1.5) is found in the works [28,47] of Karasev and Maslov.

Denote by \hat{X}_μ a set of noncommuting selfadjoint operators with smooth Weyl symbols $X_\mu(z)$. Construct operator valued functions of \hat{X}_μ in the following fashion. Let $f: \mathbb{R}^6 \rightarrow \mathbb{R}$ be a smooth function having Fourier transform \tilde{f} . Then

$$f(\hat{X}) = f(\hat{X}_1, \dots, \hat{X}_6) \equiv \int_{\mathbb{R}^6} du \tilde{f}(u) e^{iu \cdot \hat{X}} \tag{A10a}$$

defines a Weyl symmetrized function of \hat{X}_μ . In the special case where $\hat{X}_\mu = \hat{z}_\mu$, the function $f(z)$ is the symbol of $f(\hat{z})$. In Ref. [28] (cf. Appendix 1, Sec. 1.4) the following asymptotic expansion was established:

FIG. 5. y dependence of the $\gamma_t^{(0)}(p_2)$ term.

$$\begin{aligned} \sigma f(\hat{X})(z) = & f(X(z)) + \hbar^2 \left[-\frac{1}{16} B_{12}^2 \langle X_\alpha, X_\beta \rangle(z) f_{;\alpha\beta}(X(z)) \right. \\ & \left. - \frac{1}{24} B_{12} B_{23} \langle X_\alpha, X_\beta, X_\gamma \rangle(z) f_{;\alpha\beta\gamma}(X(z)) \right] \\ & + O(\hbar^4). \end{aligned} \quad (\text{A10b})$$

Now consider quantum flow. Write the observable in Weyl symmetrized form, $\hat{A} = A(\hat{z})$, i.e., $A = \sigma \hat{A} = f$. The Heisenberg-Weyl evolution is

$$\Gamma_t \sigma \hat{A} = \sigma \Gamma(t) \hat{A} = \sigma f(\Gamma(t) \hat{z}). \quad (\text{A11})$$

Apply Eq. (A10b) to $\sigma f(\Gamma(t) \hat{z})$ by setting $\hat{X}_\mu = \Gamma(t) \hat{z}_\mu$ and $X_\mu(z) = Z_\mu(t, \hbar; z)$. Employ expansion (2.8) for $Z_\mu(t, \hbar; z)$ and then Taylor expand the f functional arguments about $g(t|z)$. One immediately recovers expansion (1.5) to order $O(\hbar^2)$ and reproduces Eq. (2.11).

APPENDIX B: PHASE SPACE ROTATIONS AND TENSOR REPRESENTATIONS

The Wigner transform maps operator valued tensors on \mathcal{H} to Weyl symbol valued tensors on $T^*(\mathbb{R}^3)$. This appendix reviews the definition of these symbol valued tensors and obtains their transformation properties under rotations.

Each linear invertible coordinate transformation $Q: \mathbb{R}_q^3 \rightarrow \mathbb{R}_q^3$ defines a point canonical transformation on $T^*(\mathbb{R}^3)$ in the following fashion:

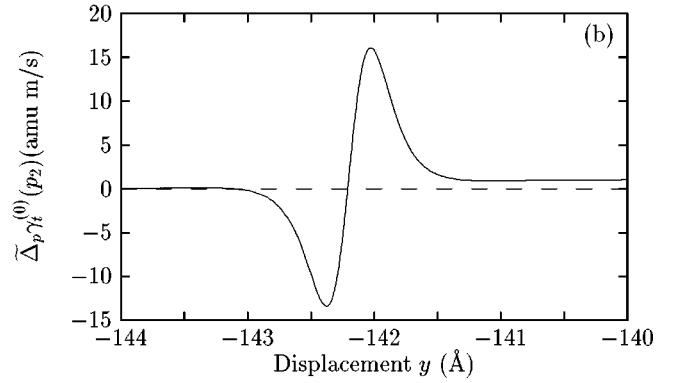
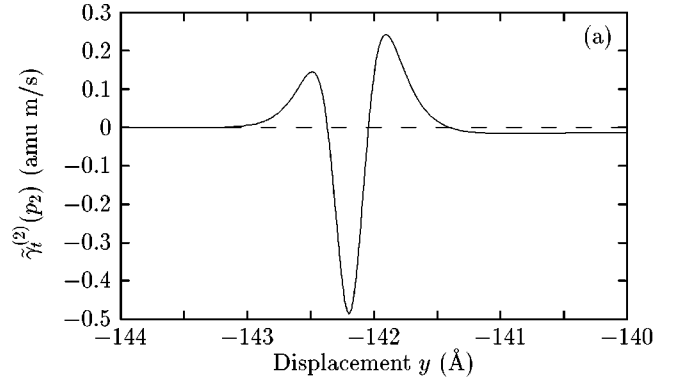
$$q' = Qq, \quad \det Q \neq 0. \quad (\text{B1})$$

The induced transformation of the momentum variable is $p' = (Q^{-1})^T p$. The combined coordinate and momentum map $z = (q, p) \mapsto z' = (q', p')$ is canonical for all Q .

Write, for arbitrary unit vector e , the e, ϕ rotation in \mathbb{R}_q^3 as $R = R_e(\phi)$. Setting $Q = R$, we note that $p' = Rp$ results as a consequence of the real orthogonal property of R . The resultant transformation $z' = \mathcal{R}z$ is a rotation in phase space. A convenient notation for \mathcal{R} is the block matrix decomposition,

$$\begin{pmatrix} q' \\ p' \end{pmatrix} = \mathcal{R} \begin{pmatrix} q \\ p \end{pmatrix}, \quad \mathcal{R} = \mathcal{R}_e(\phi) = \begin{bmatrix} R_e(\phi) & 0 \\ 0 & R_e(\phi) \end{bmatrix}. \quad (\text{B2})$$

The transformation \mathcal{R} is both a real orthogonal and a symplectic six-dimensional matrix.

FIG. 6. y dependence of the (a) $\tilde{\gamma}_t^{(2)}(p_2)$ and (b) $\tilde{\Delta}_p \gamma_t^{(0)}(p_2)$ terms.

The suitable definition of tensor operators which incorporate the phase space rotation \mathcal{R} is revealed by examining the canonical operators \hat{q} and \hat{p} . Both of these are \mathbb{R}^3 rank one tensor operators. Under the quantum rotation generated by $\hat{L} = \hat{q} \times \hat{p}$ this pair of operators transforms as

$$U^\dagger(R) \hat{z}_\mu U(R) = \mathcal{R}_{\mu\nu} \hat{z}_\nu, \quad (\text{B3})$$

where $U(R) = \exp(-i\phi e \cdot \hat{L}/\hbar)$.

A family $\{\hat{X}_{\mu_1 \dots \mu_n}\}$ of operators on $\mathcal{H} = L^2(\mathbb{R}^3)$ is defined to be a rank n phase-space tensor operator if under conjugation with $U(R)$ it transforms as

$$\hat{X}'_{\mu_1 \dots \mu_n} \equiv U^\dagger(R) \hat{X}_{\mu_1 \dots \mu_n} U(R) = \mathcal{R}_{\mu_1 \nu_1} \dots \mathcal{R}_{\mu_n \nu_n} \hat{X}_{\nu_1 \dots \nu_n}. \quad (\text{B4})$$

Taking the Wigner transform of identity (B4) just replaces the operators $\hat{X}'_{\mu_1 \dots \mu_n}, \hat{X}_{\nu_1 \dots \nu_n}$ by their corresponding symbols $X'_{\mu_1 \dots \mu_n}, X_{\nu_1 \dots \nu_n}$.

The most useful form of the symbol image of Eq. (B4) incorporates the affine covariance property [30] of the Wigner transform. In the form required here, this property states: Suppose S is a symplectic matrix and that $M(S)$ is a unitary operator obeying $M(S)^\dagger \hat{z} M(S) = S \hat{z}$. Namely, $M(S)$ is a metaplectic operator. Then the σ transform of an arbitrary \hat{A} conjugated with $M(S)$ satisfies

$$\sigma(M(S)^\dagger \hat{A} M(S))(z) = A(Sz). \quad (\text{B5})$$

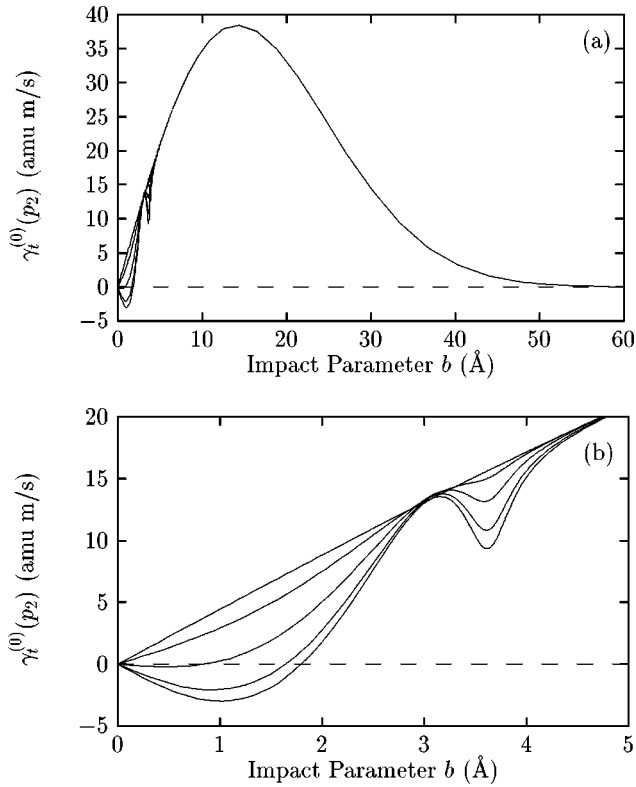


FIG. 7. (a) $\gamma_t^{(0)}(p_2)$ b functional dependence. (b) detail of (a).

Note that if we set $\mathcal{S}=\mathcal{R}$ then Eq. (B3) confirms that $U(R)$ is a metaplectic operator. Thus the covariance identity (B5) implies

$$X'_{\mu_1 \dots \mu_n}(z) \equiv \sigma(U^\dagger(R) \hat{X}_{\mu_1 \dots \mu_n} U(R))(z) = X_{\mu_1 \dots \mu_n}(\mathcal{R}z). \quad (\text{B6})$$

Combining Eqs. (B6) and (B4) establishes the Weyl symbol tensor transformation rule,

$$X_{\mu_1 \dots \mu_n}(\mathcal{R}z) = \mathcal{R}_{\mu_1 \nu_1} \dots \mathcal{R}_{\mu_n \nu_n} X_{\nu_1 \dots \nu_n}(z). \quad (\text{B7})$$

APPENDIX C: SOLUTION STRUCTURE AND CONSISTENCY CHECKS

The action of the semiclassical evolution operators $\gamma_t^{(0)}$ and $\gamma_t^{(2)}$ on the Weyl symbol of a typical observable $T_{\mu_1 \dots \mu_n}$ is often elaborate, exhibiting both a short range and long range structure in phase space. In this appendix we illustrate several examples of this behavior. Furthermore, we outline some of the consistency checks we have developed to ensure that the computed values of $\gamma_t^{(0)}$ and $\gamma_t^{(2)}$ are correct. The reported results are all for the helium atom system.

First consider the integrand of the expectation value $\langle \Gamma(t) \hat{T}_{\mu_1 \dots \mu_n} \rangle_\psi$ as a function of the variable y for fixed impact parameter b . We choose the observable to be $T_\mu = z_\mu$ with $\mu=5$, namely, the momentum coordinate function p_2 . For the trajectory with initial impact parameter $b=1.33 \text{ \AA}$ and velocity 450 m/s, the three components ($\gamma_t^{(0)}$, $\tilde{\gamma}_t^{(2)}$, $\tilde{\Delta}_p \gamma_t^{(0)}$) of the integrand in Eq. (4.7) are seen in the following two figures.

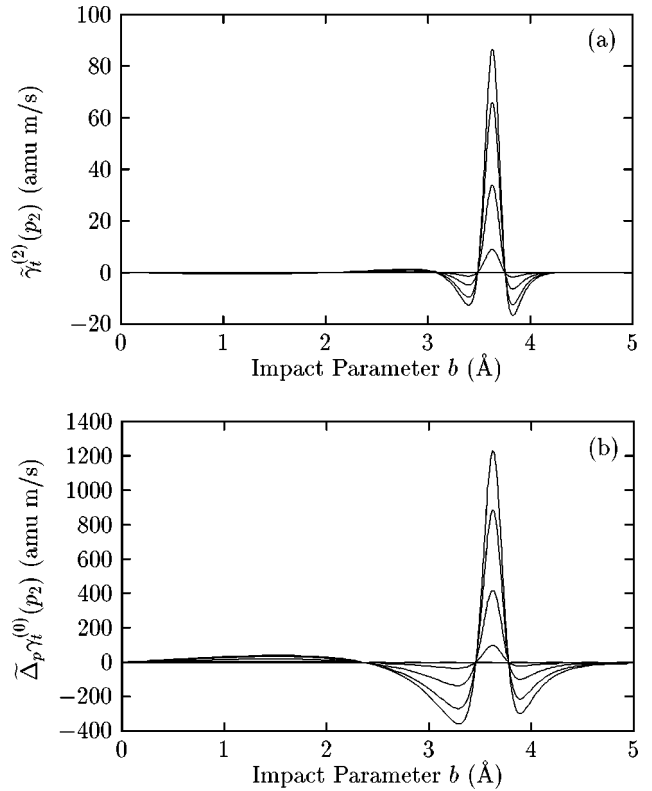


FIG. 8. (a) $\tilde{\gamma}_t^{(2)}(p_2)$ and (b) $\tilde{\Delta}_p \gamma_t^{(0)}(p_2)$ b functional dependence.

The curves in Fig. 5 show the $\gamma_t^{(0)}(p_2)$ portion of the integrand of Eq. (4.7) for five different times: 0, 0.2800, 0.3111, 0.3422, and 0.4978 (10^{-10} s). The smooth upper and lower curves denote the integrand at the precollision time 0 and the postcollision time 0.4978, respectively. The upper curve is determined solely by the Wigner function $\omega_\psi(z)$. Its slow variation is the result of the large value of D . The $\gamma_t^{(0)}(p_2)$ plot is read as follows. For the intermediate time 0.3111 the y function begins at the left on the top branch. In the region around $y = -142 \text{ \AA}$ the trajectories are undergoing active interaction with the potential and there the curve abruptly shifts to the smooth lower branch. Similar interpretations apply for the other two intermediate times.

The two curves in Fig. 6 display the y behavior of the $\tilde{\gamma}_t^{(2)}(p_2)$ and $\tilde{\Delta}_p \gamma_t^{(0)}(p_2)$ contributions for the time 0.3111.

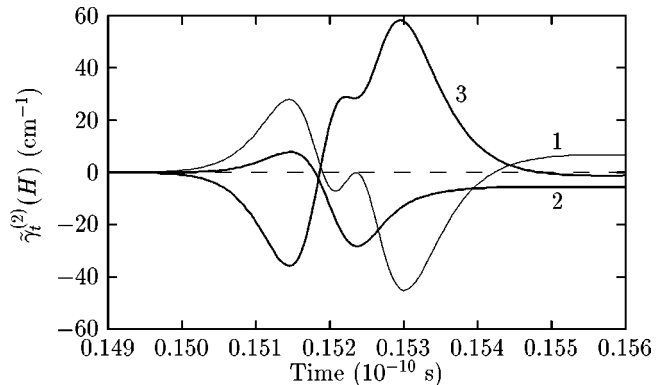


FIG. 9. Component cancellation in $\tilde{\gamma}_t^{(2)}(H)$.

TABLE VII. Consistency checks.

Time (10^{-10} s)	$\langle \gamma_i^{(0)}(H) \rangle$ (cm^{-1})	$\langle \tilde{\gamma}_i^{(2)}(H) \rangle$ (cm^{-1})	$\langle \gamma_i^{(0)}(H*L^2) \rangle$ ($10^{-20} \text{ s}^2 \text{ cm}^{-3}$)	$\langle \tilde{\gamma}_i^{(2)}(H*L^2) \rangle$ ($10^{-20} \text{ s}^2 \text{ cm}^{-3}$)
0.0000	16.938 679 5	10^{-44}	38.784 211	10^{-32}
0.1556	16.938 679 4	6.868×10^{-14}	38.784 210	3.213×10^{-9}
0.1889	16.938 679 4	1.305×10^{-11}	38.784 210	9.035×10^{-8}
0.2800	16.938 676 5	1.669×10^{-8}	38.784 204	7.774×10^{-5}
0.3111	16.938 676 6	7.407×10^{-8}	38.784 204	1.357×10^{-4}
0.3422	16.938 676 6	1.777×10^{-7}	38.784 204	9.307×10^{-5}
0.4889	16.938 676 5	2.949×10^{-7}	38.784 204	2.958×10^{-7}
0.4978	16.938 676 5	2.949×10^{-7}	38.784 204	2.956×10^{-7}

There are similar rapid variations of these quantities for the times 0.2800 and 0.3422.

Our computation of the expectation value (4.7) first completes the y integration and then carries out the integral over the impact parameter. For the same observable p_2 , the b -dependent components of Eq. (4.7) are displayed in Figs. 7 and 8.

The pair of curves in Fig. 7 describes the $\gamma_i^{(0)}$ contribution on two different b scales. The near coincidence of the five curves occurs at the forward glory scattering value $b = 3.06 \text{ \AA}$. The subsequent maximum set of deflections occurs for the rainbow scattering at $b = 3.62 \text{ \AA}$. The associated maximum angle of deflection is -0.93 radians measured relative to the y axis. The next pair of curves in Fig. 8 are the $\tilde{\gamma}_i^{(2)}(p_2)$ and $\tilde{\Delta}_p \gamma_i^{(0)}(p_2)$ contributions, respectively. Again their maximum values are concentrated in the impact parameter region near the glory and rainbow values of the impact parameter. As time increases the values of $\tilde{\gamma}_i^{(2)}(p_2)$ and $\tilde{\Delta}_p \gamma_i^{(0)}(p_2)$ grow.

In order to integrate accurately over the fine structure in both b and y variables it is necessary to have a large number of integration points in both these dimensions. Here and in the tables of results listed in Sec. V we have used 250 points in the y variable and 130 points in the b variable. These static mesh points cover the region in phase space that supports the Wigner function $\omega_\psi(z)$.

In view of the fact that the operator $\gamma_i^{(2)}$ is the final result

of a four stage hierarchical calculation it is worthwhile to establish its correctness via a series of consistency checks. One of the most effective of these involves observables that are simultaneously classical and quantum constants of motion. In this case exact results are known. Obvious choices are $\hat{H}, \hat{L}^2, \hat{L}_3$. Furthermore, one can form additional constants of motion from the products of these operators. Consider the product $\hat{H}\hat{L}^2$ whose symbol is $H*L^2$. Since $\Gamma_i(H*L^2) = \text{const}$ one has

$$\tilde{\gamma}_i^{(2)}(H*L^2) = \gamma_0^{(2)}(H*L^2) = 0. \quad (\text{C1})$$

The symbol $H*L^2$ is a phase space function with an elaborate structure. Numerically verifying Eq. (C1) is a demanding check on accuracy and consistency of $\gamma_i^{(2)}$. Figure 9 and Table VII show this consistency.

The three time dependent curves here are the $z^{(2)}$, $w_{\alpha\beta}$, and $w_{\alpha\beta\gamma}$ components of $\tilde{\gamma}_i^{(2)}(H)$ [labeled 1,2,3 in Fig. 9] evaluated along a trajectory with initial data $b = 2.27 \text{ \AA}$, $y = -70 \text{ \AA}$, and velocity 450 m/s. The cancellation of their sum to zero is accurate to at least seven digits. Table VII displays the quantum average of \hat{H} and $\hat{H}\hat{L}^2$ at eight different times. The deviation of the average values of $\tilde{\gamma}_i^{(2)}(H)$ and $\tilde{\gamma}_i^{(2)}(H*L^2)$ from zero is a measure of the accumulated error in our numerical calculations. It is always extremely small relative to the scale set by the $\gamma_i^{(0)}$ terms. More consistency checks are described by McQuarrie [48].

-
- [1] J. E. Moyal, Proc. Cambridge Philos. Soc. **45**, 99 (1949).
[2] H. J. Groenewold, Physica (Amsterdam) **12**, 405 (1946).
[3] T. Takabayasi, Prog. Theor. Phys. **11**, 341 (1954).
[4] G. A. Baker, Jr., Phys. Rev. **109**, 2198 (1958).
[5] D. B. Fairlie, Proc. Cambridge Philos. Soc. **60**, 581 (1964).
[6] J. C. T. Pool, J. Math. Phys. **7**, 66 (1966).
[7] K. İmre, E. Özizmir, M. Rosenbaum, and P. F. Zweifel, J. Math. Phys. **8**, 1097 (1967).
[8] A. Grossmann, G. Loupias, and E. M. Stein, Ann. Inst. Fourier **18**, 343 (1968).
[9] F. A. Berezin and M. A. Šubin, in *Proceedings of the Colloquia Mathematica Societatis János Bolyai, 5. Hilbert Space Operators*, edited by B. Szokefalvi-Nagy (North-Holland, Amsterdam, 1972), p. 21.
[10] S. R. DeGroot and L. G. Suttrop, *Foundations of Electrodynamics* (North-Holland, Amsterdam, 1972).
[11] F. A. Berezin, Izv. Akad. Nauk SSR Ser. Fiz. Mat. Nauk **38**, 363 (1974).
[12] A. Grossmann, Commun. Math. Phys. **48**, 191 (1976).
[13] M. A. Antonets, Moscow Univ. Math. Bull. **32(6)**, 21 (1977).
[14] M. A. Antonets, Lett. Math. Phys. **2**, 241 (1978).
[15] A. Royer, Phys. Rev. A **15**, 449 (1977).
[16] M. V. Berry, Philos. Trans. R. Soc. London, Ser. A **287**, 237 (1977).
[17] T. B. Smith, J. Phys. A **11**, 2179 (1978).
[18] A. Voros, J. Funct. Anal. **29**, 104 (1978).
[19] F. Bayen *et al.*, Ann. Phys. (N.Y.) **111**, 61 (1978).
[20] M. S. Marinov, J. Phys. A **12**, 31 (1979).

- [21] R. T. Prosser, *J. Math. Phys.* **24**, 548 (1983).
- [22] P. Carruthers and F. Zachariasen, *Rev. Mod. Phys.* **55**, 245 (1983).
- [23] F. J. Narcowich, *J. Math. Phys.* **27**, 2502 (1986).
- [24] D. Robert, *Autour de l'Approximation Semi-Classique* (Birkhauser, Boston, MA, 1987).
- [25] G. B. Folland, *Harmonic Analysis in Phase Space* (Princeton University Press, Princeton, New Jersey, 1989).
- [26] R. Estrada, J. M. Gracia-Bondía, and J. C. Varilly, *J. Math. Phys.* **30**, 2789 (1989).
- [27] M. S. Marinov, *Phys. Lett. A* **153**, 5 (1991).
- [28] M. V. Karasev and V. P. Maslov, *Nonlinear Poisson Brackets* (American Mathematical Society, Providence, Rhode Island, 1991).
- [29] I. Borsari and S. Graffi, *J. Math. Phys.* **35**, 4439 (1994).
- [30] T. A. Osborn and F. H. Molzahn, *Ann. Phys. (N.Y.)* **241**, 79 (1995).
- [31] E. P. Wigner, *Phys. Rev.* **40**, 749 (1932).
- [32] H. Weyl, *Z. Phys.* **46**, 1 (1927).
- [33] L. Hörmander, *Commun. Pure Appl. Math.* **32**, 359 (1979).
- [34] D. Bambusi, S. Graffi, and T. Paul (unpublished).
- [35] F. H. Molzahn and T. A. Osborn, *Ann. Phys. (N.Y.)* **230**, 343 (1994).
- [36] M. E. Rose, *Elementary Theory of Angular Momentum* (Wiley, New York, 1957).
- [37] J. de Boer and A. Michels, *Physica (Amsterdam)* **5**, 945 (1938).
- [38] J. O. Hirschfelder, C. F. Curtis, and R. B. Bird, *Molecular Theory of Gases and Liquids* (Wiley, New York, 1954).
- [39] B. E. Fender and G. D. Halsey, *J. Chem. Phys.* **36**, 1881 (1962).
- [40] R. Seydel, *From Equilibrium to Chaos* (Elsevier, New York, 1988).
- [41] G. L. Zaslavski, *Phys. Rep.* **80**, 157 (1981).
- [42] B. Eckhardt, *Phys. Rep.* **163**, 205 (1988).
- [43] P. W. O'Connor, S. Tomsovic, and E. J. Heller, *J. Stat. Phys.* **68**, 131 (1992).
- [44] M. Combescure and D. Robert, *Asymptotic Analysis* **14**, 377 (1997).
- [45] V. P. Maslov and M. V. Fedoriuk, *Semiclassical Approximation in Quantum Mechanics* (Reidel, Dordrecht, 1981).
- [46] M. C. Gutzwiller, *Chaos in Classical and Quantum Mechanics* (Springer-Verlag, New York, 1990).
- [47] M. V. Karasev, *Mat. Zametki* **26**, 885 (1979).
- [48] B. R. McQuarrie, Ph.D. thesis, The University of Manitoba, 1997 (unpublished).